

REPORT DOCUMENTATION PAGE				Form Approved OMB No. 0704-0188	
Public reporting burden for this collection of information is estimated to average 1 hour per response, including the time for reviewing instructions, searching existing data sources, gathering and maintaining the data needed, and completing and reviewing the collection of information. Send comments regarding this burden estimate or any other aspect of this collection of information, including suggestions for reducing the burden, to Department of Defense, Washington Headquarters Services, Directorate for Information Operations and Reports (0704-0188), 1215 Jefferson Davis Highway, Suite 1204, Arlington, VA 22202-4302. Respondents should be aware that notwithstanding any other provision of law, no person shall be subject to any penalty for failing to comply with a collection of information if it does not display a currently valid OMB control number. PLEASE DO NOT RETURN YOUR FORM TO THE ABOVE ADDRESS.					
1. REPORT DATE (DD-MM-YYYY) 31-Jan-2006		2. REPORT TYPE Final Report		3. DATES COVERED (From – To) 1 August 2005 - 01-Aug-06	
4. TITLE AND SUBTITLE Effect of Strain Rate on Ductile Fracture			5a. CONTRACT NUMBER FA8655-05-1-3049		
			5b. GRANT NUMBER		
			5c. PROGRAM ELEMENT NUMBER		
6. AUTHOR(S) Professor Wojciech K Nowacki			5d. PROJECT NUMBER		
			5d. TASK NUMBER		
			5e. WORK UNIT NUMBER		
7. PERFORMING ORGANIZATION NAME(S) AND ADDRESS(ES) Institute for Fundamental Technological Research of the Polish Academy of Sciences Swietokrzyska 21 Warsaw 00-049 Poland				8. PERFORMING ORGANIZATION REPORT NUMBER N/A	
9. SPONSORING/MONITORING AGENCY NAME(S) AND ADDRESS(ES) EOARD PSC 821 BOX 14 FPO 09421-0014				10. SPONSOR/MONITOR'S ACRONYM(S)	
				11. SPONSOR/MONITOR'S REPORT NUMBER(S) GRANT 05-3049	
12. DISTRIBUTION/AVAILABILITY STATEMENT Approved for public release; distribution is unlimited.					
13. SUPPLEMENTARY NOTES					
14. ABSTRACT This report results from a contract tasking Institute for Fundamental Technological Research of the Polish Academy of Sciences as follows: The effect of strain rate on ductile fracture is one of the least understood phenomena in modern fracture mechanics. At the same time, information on ductile fracture under dynamic loading is very important for reliable prediction of fracture and fragmentation of high-consequence structures. High-consequence structures are understood here as components of turbofan engines for fixed-wing aircraft and/or rotorcraft dynamic components. A comprehensive theoretical, experimental, and numerical research project will be undertaken to resolve some of the fundamental issues and construct a dynamic fracture locus suitable for engineering applications and implementation into the FE codes. It is envisioned that the project will be broken into three interrelated tasks: Hopkinson bar tensile fracture tests on small, flat specimens using a unique apparatus developed at IPPT; Drop tower fracture tests on specially designed specimens subjected to a combined shear/compression and shear/tension loading; Finite element simulation of dynamic experiments and construction of the dynamic fracture envelope for a few typical materials. The second and third task will be a joint endeavour between IPPT and MIT where the funding for the work at MIT will come from GE Global Research Center and the funding for the IPPT will come from this grant. No government furnished equipment or data will be used by the researchers at IPPT.					
15. SUBJECT TERMS EOARD, Fracture mechanics, Finite Element Methods, Ductile Materials					
16. SECURITY CLASSIFICATION OF:			17. LIMITATION OF ABSTRACT UL	18. NUMBER OF PAGES 75	19a. NAME OF RESPONSIBLE PERSON JOAN FULLER
a. REPORT UNCLAS	b. ABSTRACT UNCLAS	c. THIS PAGE UNCLAS			19b. TELEPHONE NUMBER <i>(Include area code)</i> +44 (0)20 7514 3154

**Report
of the**

Award No FA 8655-05-1-3049

from the European Office of Aerospace Research and Development

**“EFFECT OF STRAIN RATE ON DUCTILE
FRACTURE”**

Wojciech K. NOWACKI - principal investigator
Stefan P. GADAJ
Jerzy LUCKNER
Zdzisław NOWAK
Piotr PERZYNA
Ryszard B. PECHERSKI

*Institute of Fundamental Technological Research, Polish Academy of Sciences (IPPT)
Świętokrzyska 21, 00-049 Warsaw, Poland
e-mail: wnowacki@ippt.gov.pl*

Warsaw, January 2006

CONTENTS

1. Introduction
2. New shear fracture tests on small, flat specimens using a unique apparatus developed at IPPT, by W.K. Nowacki, J. Luckner and S.P. Gadaj
 - 2.1. Quasi-static tests in simple shear
 - 2.2. Dynamic tests in simple shear at high strain rates
 - 2.3. Metallurgical observations
 - 2.4. Dynamic tests in simple shear at very high strain rates
 - 2.5. Comparison of simple shear test with compression test
3. Constitutive model in application for finite element simulation of dynamic experiments and construction of the dynamic fracture locus, by R.B. Pęcherski, Z. Nowak, P. Perzyna
 - 3.1. Constitutive description of inelastic deformation in application for the study of strain rate effect on ductile fracture
 - 3.2. Conclusions

References
4. Annex I – PP - presentation – seminar at MIT
5. Annex II – Micromechanics of localized fracture phenomena in inelastic solids – by Z. Nowak, P. Perzyna and R.B. Pęcherski

1. Introduction

The effect of strain rate on ductile fracture is one of the least understood phenomena in modern fracture mechanics. At the same time, information on ductile fracture under dynamic loading is very important for reliable prediction of fracture and fragmentation of high-consequence structures. High-consequence structures are understood here as components of turbofan engines for fixed-wing aircraft and/or rotorcraft dynamic components. The high strain rate experiments to fracture are conducted with equipment available at the Institute of Fundamental Technical Research.

Mechanical and thermomechanical behavior of materials (DH-36 steel) applied in airplanes and helicopters, subjected to compression, tensile and simple shear tests in wide spectrum of the strain rates ($10^{-3} \text{ s}^{-1} \div 10^4 \text{ s}^{-1}$) are investigated. The tensile, cycling and shear properties seems to be very important, since the aircraft materials are subjected to such a loading during their application. The simple shear test of the DH-36 steel sheets in the case of quasi-static case as well as in the high strain rates is performed. In this kind of test (proposed by W.K. Nowacki [1]) a considerable homogeneity of the permanent strain field at finite deformations over the total length of the specimens is observed in experiments of simple shear and in the results of simulation – cf. [2]. The proposed method is the only known test providing, in the case of a thin sheet, homogeneous stress and strain fields in both the dynamic and static tests. Simple shear test is particularly attractive, since the application of this type of loading path can result in large strains without the occurrence of plastic instability. The shear tests on small, flat specimens using are described in the Chapter 2. The mechanical characteristics and the temperature distributions of the sample surface obtained by a thermovision camera during the deformation processes are recorded, processed and stored in the computerized registration system. The computer results are available for further analysis; its later reproduction in the most convenient is being possible. Investigation of the initiation and further development of fracture locus at various strain rates using the infrared technique are performed. Identification of the beginning of plastic deformation, based upon the temperature measurements, in the materials subjected to subsequent shear deformation are carried out.

The objective of the Chapter 3 is to discuss very efficient procedure of the numerical investigation of localized fracture in inelastic solids generated by impact-loaded adiabatic processes. Particular attention is focused on the proper description of a ductile mode of fracture propagating along the shear band for high impact velocities. This procedure of investigation is based on utilization the finite element method and ABAQUS system for regularized thermo-elasto-viscoplastic constitutive model of damaged material. A general constitutive model of thermo-elasto-viscoplastic damaged polycrystalline solids with a finite set of internal state variables is used. The set of internal state variables consists of two scalars, namely equivalent inelastic deformation and volume fraction porosity. The equivalent inelastic deformation can describe the dissipation effects generated by viscoplastic flow phenomena and the volume fraction porosity takes into account the microdamage evolution effects. The relaxation time is used as a regularization parameter. Fracture criterion based on the evolution of microdamage is assumed.

As a numerical example we consider dynamic simple shearing and localized fracture in thin plate. The impact loading is simulated by a velocity boundary condition which are the results of dynamic contact problem. The separation of the projectile from the specimen, resulting from wave reflections within the projectile and the specimen, occurs in the phenomenon.

A thin shear band region of finite width which undergoes significant deformation and temperature rise has been determined. Its evolution until occurrence of final fracture has been simulated. Shear band advance, shear band velocity and the development of the temperature field as a function of time have been determined. Qualitative comparison of numerical results with experimental observation data has been presented. The numerical results obtained have proven the usefulness of the thermo-elasto-viscoplastic theory in the investigation of dynamic shear band propagations and localized fracture.

In Chapter 3 an application of certain particular model of viscoplasticity, in which a multiscale mechanism of shear banding is accounted for, is presented. Also a possible method of identification of this model is discussed. The identification of the proposed model can be based on the experimental results presented in [15]. The presented model can be applied for the analysis of strain rate effect on ductile fracture of DH-36 steel with use of the original methodology developed by T. Wierzbicki and coworkers, cf. eg. [16].

2. New shear fracture tests on small, flat specimens using a unique apparatus developed at IPPT

In the static investigations of thin sheets we can distinguish two approaches, based on different principles of the shear device. The first type of shear device of the one-shear zone only, proposed by G'Sell et al. [3], has been performed for the investigation of thin polymer sheets in the conditions of static shear. The principle of this construction has been adopted for testing of the steel sheets, Tourabi et al. [4] and Rauch and G'Sell [5], cyclic shear of metallic sheets, Wack et Tourabi [6] and for the shape-memory alloy, Manach and Favier [7]. In the second type of device for the static tests (see Fig. 1), Yoskida & Myauchi [8], the „double-shear” specimen is applied. It is a specimen with two zones of shear. The fundamental attribute of this device is its symmetry with respect to the direction of loading. Both the above experimental techniques have their advantages and the inconveniences. In the first method, proposed by G'Sell, one can obtain a uniform zone of the deformation field. First of all, it is possible in this method to select one direction in which we can examine the behavior of material. The symmetry of loading may need special very sophisticated carriages. The second method, proposed by Myauchi, is the simplest in use. In this method, the rigorous conditions of symmetry may be fulfilled. The exact fixation in grips must be assured. The inconvenience of this method is the fact that the homogeneity of the deformation field is not very good, compared with the first method. The free boundaries of the specimen have the influence for the field of deformations and stresses.

In the case of dynamic loading, using the Kolsky bar, also called a Split Hopkinson Pressure Bar (SHPB), the scheme of the shear device (see Fig. 1) proposed by Myauchi, is more convenient for this kind of test. Regarding the miniature of the shear device, the scheme with horizontal and vertical carriages, proposed by G'Sell, is practically unfeasible. A new shear device was used by Gary and Nowacki [1] to perform tests under high strain rates on specimens having the form of slabs, such as metal sheets. The loading and the displacements of this device are controlled by a Split Hopkinson Pressure Bar acting in compression. The role of the special device is to transform the compression into a plane shear (as in the Myauchi system). The dynamic simple shear tests so obtained is the only known method allowing to obtain a very good homogeneity of the residual strain field over the total length of

the specimen, without localization of the deformations, as in the case of torsion of thin-walled tubes, Marchand and Duffy [9].

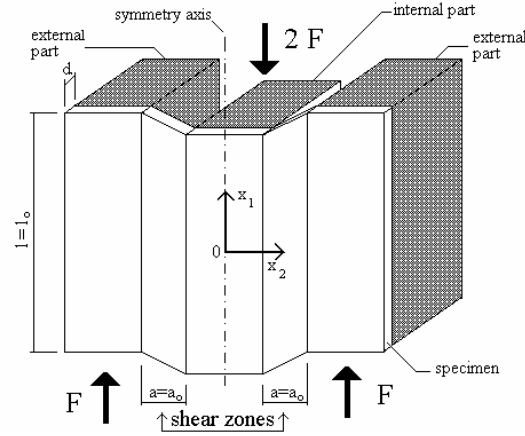


Figure 1. Scheme of shear testing; two shear zones

The shear device for investigations at high strain rates consists of two coaxial cylindrical parts, namely the external tubular part and the internal massive part (see Fig. 2). Both cylinders are divided into two symmetrical parts, and between them the sheet to be tested is fixed.



Figure 2. Shear device

Two boundaries of the specimen between the internal and external parts of the device are in plane shear when these cylinders move axially one toward the other. Each shear zone before test is rectangular and becomes very close to a parallelogram having a constant length and a constant height (see Fig. 1 and Fig. 3).

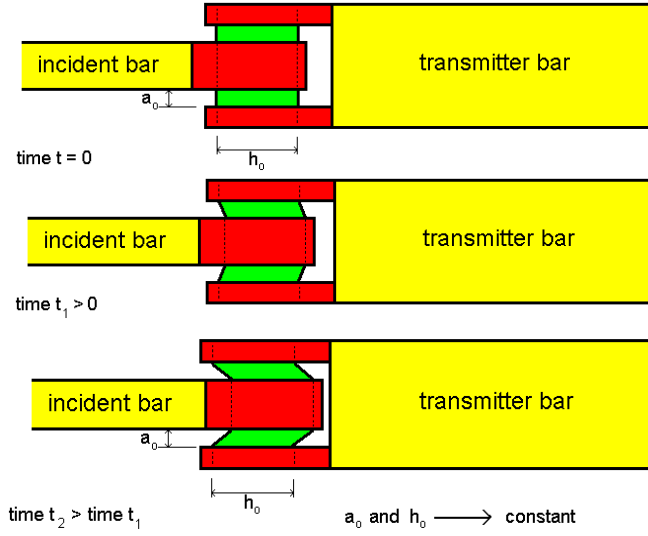


Figure 3. Scheme of simple shear. Loading and displacement are controlled by a SHPB acting in compression

The greatest double-shear specimen height allowed by the shear device is $l_o = 30$ mm. The width value a_o is chosen with a view to satisfying two requirements: first the ratio a_o/d of the width to the thickness has to be small enough to avoid buckling of the sheared zone ($a_o/d < 10$) and secondly, the ratio a_o/l_o of the width to the height has to be sufficiently small to minimize the error due to the no homogeneity of the shear stress and strain at the two ends of the sample ($a_o/l_o < 1/10$), Tourabi et al. [4] and Gary and Nowacki [1]. In our case, the material sheet has a nominal thickness of 0.64 mm (usually specimens can have different thickness). In our experimental investigations we used specimens made of DH-36 steel. We apply in our quasi-static tests the ratio $a_o/l_o = 1/10$ (the width of the shear zone a_o is constant and equal to 3mm; $a_o/d = 4.7$). In the case of dynamic test at high strain rates we use specimens of the strain gauge length 20mm [10]. Design of the specimen for dynamic testing in simple shear is presented on the Fig. 4.

It is important to mention that we use our shear device in a large range of strain rates: in the case of quasi-static tests from 10^{-3} s^{-1} , to 10^3 s^{-1} in the case of dynamic tests at high strain rates. Using the same shear device in all experiments, we can obtain a conviction of the reliability of our experimental results.

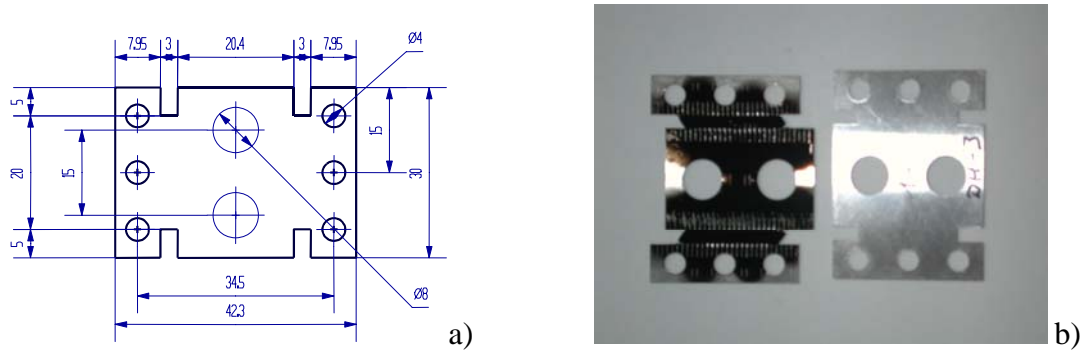


Figure 4. Specimen used during double shear tests. On the figure b) specimen after and before simple shear deformation

2.1. Quasi-static tests in simple shear. Deformation processes always modify the temperature fields in materials while the temperature variations influence the stress-strain characteristic. Strong effects of the thermomechanical coupling are observed during the process of the simple shear test. During this test the first invariant of stress tensor $\Delta\sigma_{ii} = 0$, thus, in elastic range of deformation temperature does not change [11]. The following plastic deformation is accompanied by increase in temperature. It is caused by transformation of a significant part of the plastic energy into heat [12].

The goal of our investigation was obtaining the mechanical curves as well as the temperature distributions in the shear areas and comparison them in order to analyse the processes of materials deformation. The samples were placed in a specially designed grip for quasi-static tests, transforming the compression into a simple shear process (see Fig. 5). The grip was fitted in the testing machine, working in compression mode. A change of temperature of the surface of two shear paths has been observed during the test using an infrared camera.

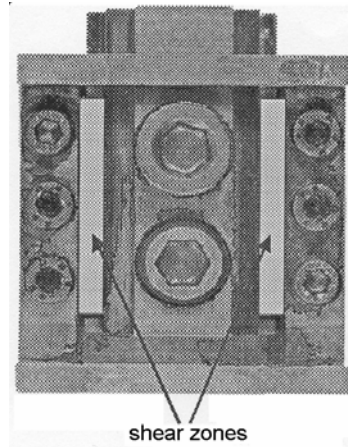


Figure 5. Photograph of shear test device

The tests were performed at room temperature (295 K), with the rates of deformation equal to 10^{-3} s^{-1} , 10^{-1} s^{-1} and 10^0 s^{-1} .

During deformation, the load vs. crosshead displacement and the distribution of infrared radiation, emitted by the specimen, were continuously registered. The distribution was measured using the thermovision camera coupled with a computer system of data acquisition and conversion.

The mechanical characteristics made it possible to derive the stress-strain relations. The distribution of intensity of the infrared radiation registered in the same time allowed us to reconstruct thermal pictures (Fig. 6) of the samples and in this way to find the temperature changes of the sample subjected to shear test. The increments of the sample's temperature were calculated as an average value from the central segments along the sheared zones. This approach let us to compare the mechanical and the thermal characteristics, and then to find temperature–stress relations $\Delta T(\sigma_{12})$.

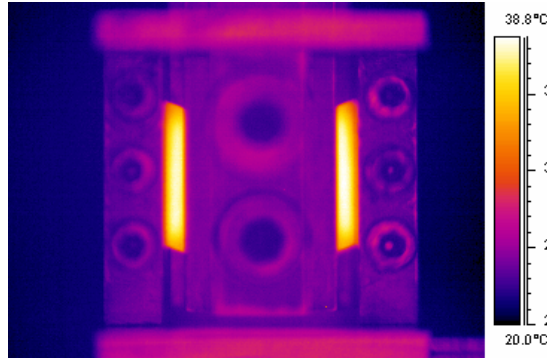


Figure 6. Example of thermogram obtained during simple shear test of DH-36 steel

The mean-square error of temperature evaluation was about $0.2 \div 0.5$ K. In order to ensure higher and more homogeneous emissivity, the surfaces of the shear zones of the steel sheet specimens were blackened with a carbon powder.

As results of the study we have obtained stress-strain and temperature-strain characteristics. Example of these stress-strain relations obtained for DH-36 steel deformed with shear rate equal to 10^{-3} s^{-1} , 10^{-1} s^{-1} and 10^0 s^{-1} are presented in Figs. 7a, b and c respectively and temperature-strain relations are given in Figs. 8a and b, for strain rates 10^{-1} s^{-1} and 10^0 s^{-1} .

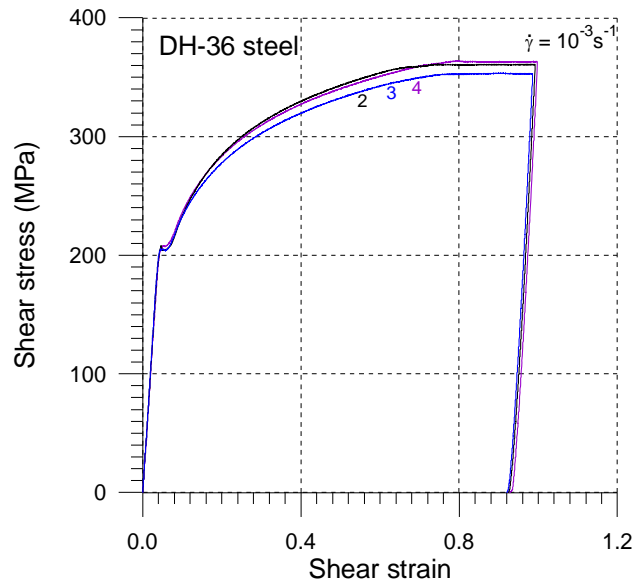


Figure 7a. Stress-strain relation obtained during simple shear of DH-36 steel with shear rate equal 10^{-3} s^{-1} ; 2,3,4 – tests numbers

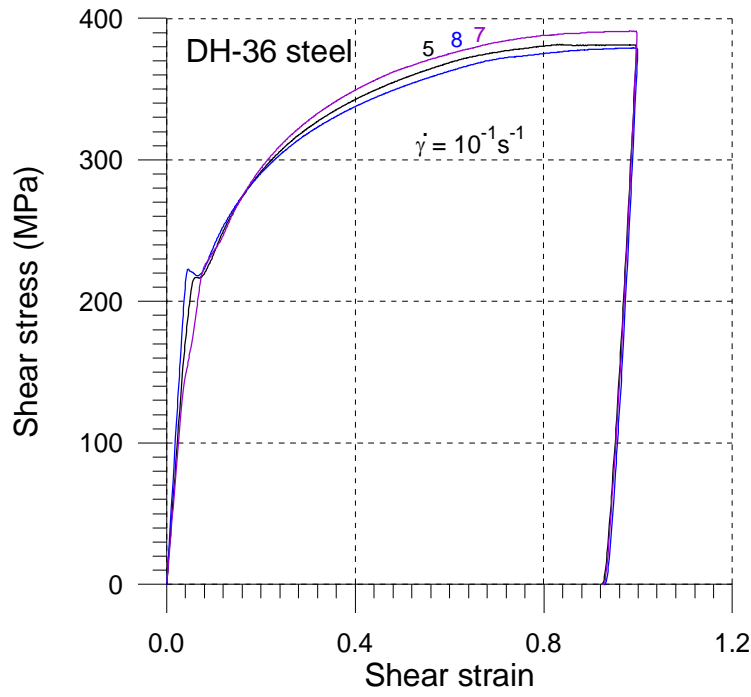


Figure 7b. Stress-strain relation obtained during simple shear of DH-36 steel with shear rate equal 10^{-1} s^{-1} ; 5,7,8 – tests numbers

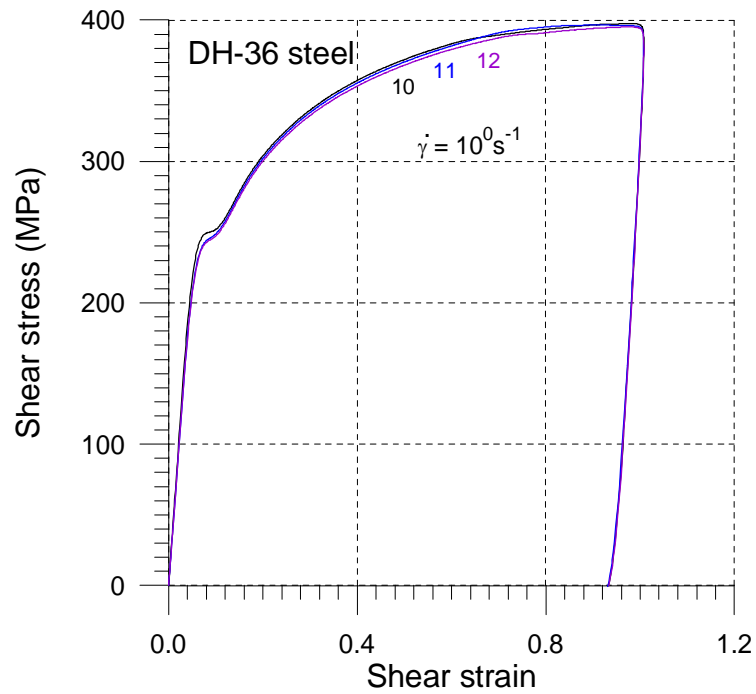


Figure 7c. Stress-strain relation obtained during simple shear of DH-36 steel with shear rate equal 10^0 s^{-1} ; 10,11,12 – tests numbers

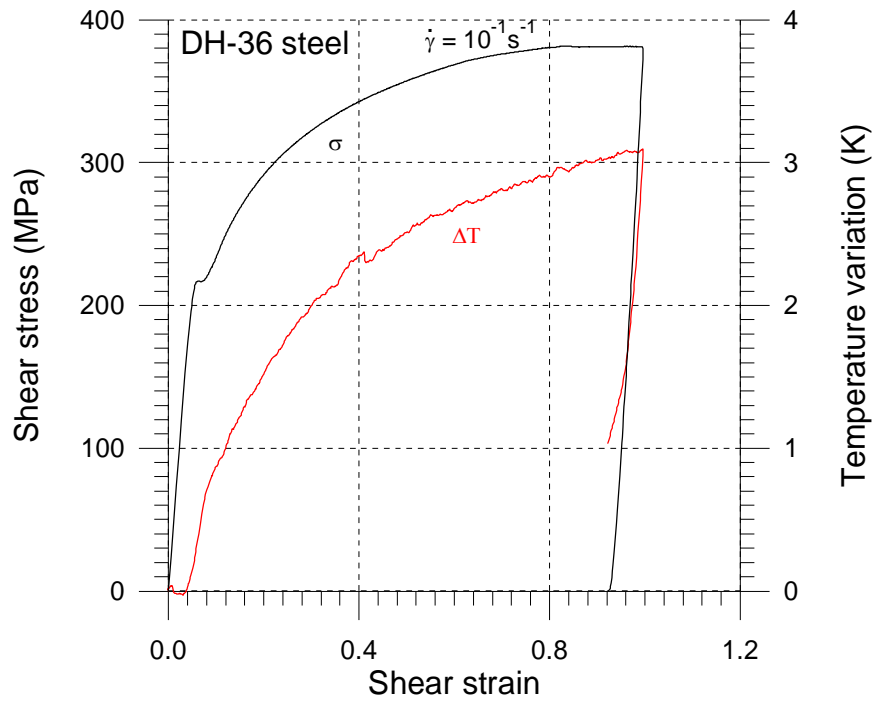


Figure 8a. Stress-strain and mean temperature changes curves of DH-36 steel at the rate of deformation equal 10^{-1} s^{-1}

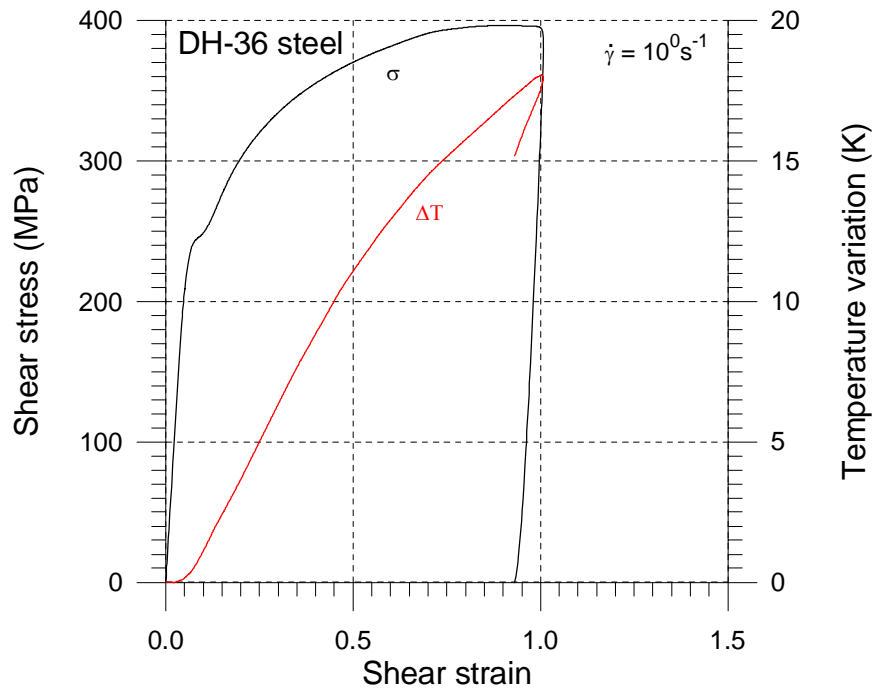


Figure 8b. Stress-strain and mean temperature changes curves of DH-36 steel at the rate of deformation equal 10^0 s^{-1}

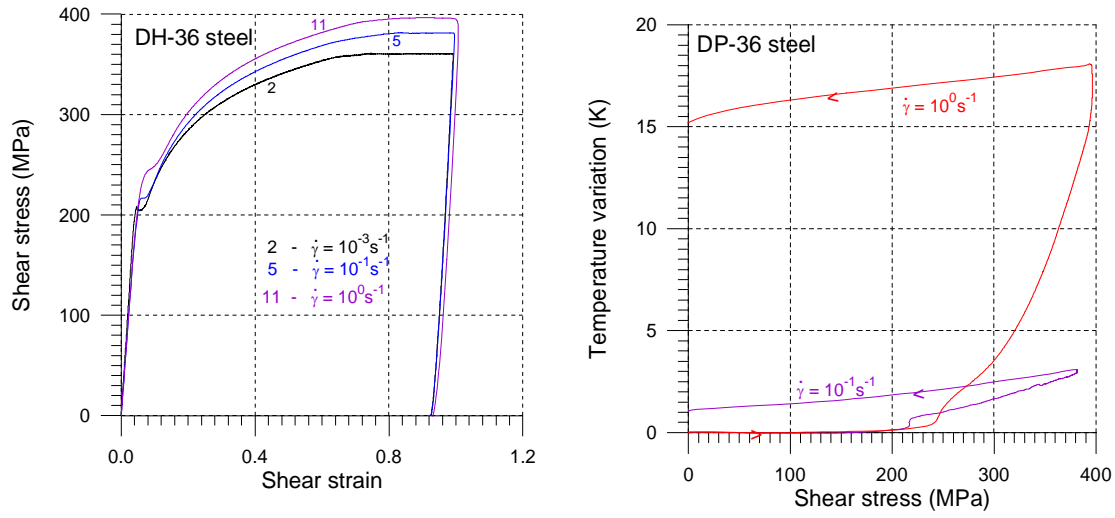


Figure 9 a). Stress-strain relation obtained during simple shear of DH-36 steel with different strain rate; 2,5,11 – tests numbers. b) Stress dependence of mean temperature change for various strain rates of DH-36 steel; temperature does not vary with the rate of deformation equal 10^{-3} s^{-1} .

For the DH-36 steel, temperature does not change in elastic range of shear, i.e. any thermoelastic effect was observed. The rapid increments of temperature are observed in the region of plastic deformation. The temperature increases with increase of the rate of deformation. During unloading, the temperature smoothly decreases due to the heat transmission to the grips and surroundings.

2.2. Dynamic tests in simple shear at high strain rates. The device with double-shear specimen is placed between two bars of the SHPB (Fig. 10). The mechanical impedance of the shear device and the SHPB must be the same to avoid the noise in the interface signal. The impulse is created by the third projectile bar: the usual compression technique. The impact velocity is measured by the set-up consisting of three sources of light and three independent photodiodes. The time interval during crossing of a projectile by two rays of light is recorded by the time counter. We have to register the input, the transmitted and the reflected impulses: ε_i , ε_t and ε_r – cf. Fig. 11. Impulses are registered at the strain resistance gauges.

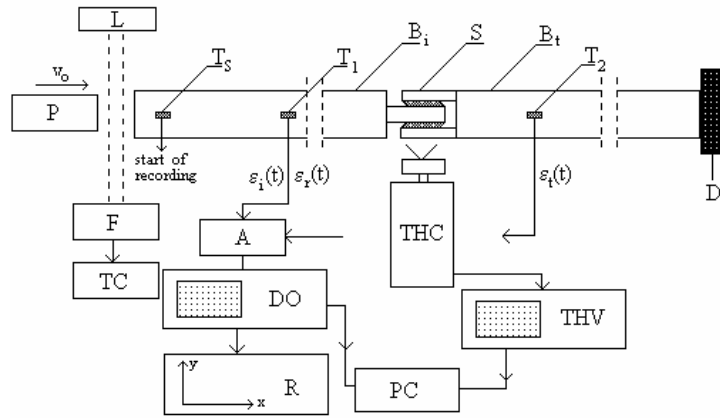


Figure 10. Standard SHPB apparatus. P - projectile, B_i - incident bar, B_t - transmitting bar, S - shear device with double shear specimen, D - damper, L - source of light, F - photodiodes, TC - time counter, T_1 , T_2 and T_s - strain gauges, A - amplifier, DO - digital oscilloscope, PC - microcomputer, R - xy recorder or graphic printer, THC - thermovision camera, THV - oscilloscope of thermovision set

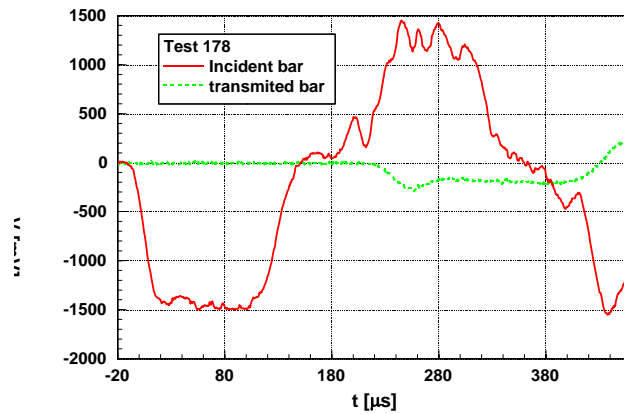


Figure 11. Incident, reflected and transmitted waves

The specimen is deformed not only between the grips, in the gauge section. The part under the grips is partially deformed too. The transversal strike lines, marked on the specimen before the test, become after deformation the curves with the strike sections – Fig. 12a.

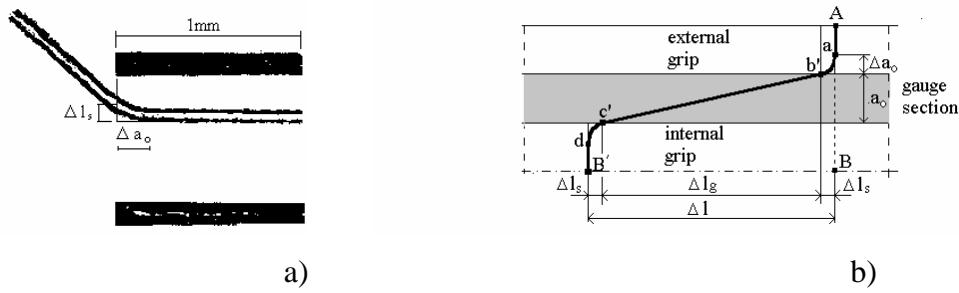


Figure 12. Displacement between external and internal grips

Relative displacement of external and internal parts of the shear device Δl is a sum of two terms: $\Delta l = \Delta l_g + 2 \Delta l_s$, where Δl_g corresponds to the deformation in the simple shear defined as $\gamma = \Delta l_g / a_o$, and Δl_s correspond to the value of sliding under the grips.

At the first step, the shear device together with the universal testing machine has been used under quasi-static loading for the verification. Measurements of the displacement or deformations must be precise.

It was assumed that in the simple shear, there is no change in the cross section: $S_E = l_o$ $d = \text{const}$. Then the mean shear stress is defined by $\sigma_{12} = F/2 S_E$. The estimates of the sliding value under the grips Δl_s can be obtained in the quasi-static test of loading unloading. After such a test, the permanent deformation of the specimen can be measured using an optical microscope. Comparison of the optical measurement with those obtained by displacement at the end of the unloading process yields the value of Δl_s . This procedure must be repeated for the given range of shear deformations γ .

Sliding values under the grips (Δl_s), after quasistatic simple shear up to 100% deformation and unloading, for test with different strain rate are shown in Table 1. Three specimens were used to obtain the average value for every rate of deformation. For every specimen three lines were taken to obtain this value (see Fig. 13.)

Table 1

Strain rate	Δl_s (mm)
10^{-3}	0.30
10^{-1}	0.32
10^0	0.35

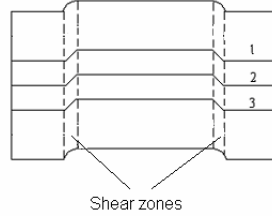


Figure 13. The transversal strike lines on the specimen applied to measure changes of geometry of the shear zones according to the method shown in the Fig.12.

For the DH-36 steel significant part of deformation take place out of the shear zones – under the grips. In the quasistatic range of deformation, the contribution of sliding under grips increases a little when the shear deformation increases.

Average value of the deformation range out of shear zone was $\Delta a_0 = 0.52$ mm (see Fig. 12). This value was not changed with rate of deformation.

Measurement of dynamic deformation at high strain rates in the case of simple shear of the metal sheets is more complicated as in the quasi-static loading. In the case of dynamic deformation with the SHPB, determination of the relative displacement Δl of the external and internal parts of the shear device is not a quite simple matter. It is assumed that both bars are elastic and displacements $\delta_l(t)$ and $\delta_2(t)$ of two faces of the shear device can be determined from the measured elastic waves ε_i , ε_l and ε_r :

$$(2.1) \quad \delta_1(t) = c_o \int_0^t [\varepsilon_i(\tau) - \varepsilon_r(\tau)] d\tau, \quad \delta_2(t) = c_o \int_0^t \varepsilon_l(\tau) d\tau,$$

where c_o is the longitudinal wave speed in the bars.

The mean shear strain $\bar{\gamma}^*$ corresponding to a relative displacement of two parts of

$$(2.2) \quad \bar{\gamma}^* = \frac{\Delta l}{a_o} = \frac{1}{a_o} [\delta_1(t) - \delta_2(t)]$$

Now one must take into account the displacement correction due to the sliding of the specimen under the grips. The mean shear strain $\bar{\gamma}^*(t)$ can be expressed as

$$(2.3) \quad \bar{\gamma}(t) = \bar{\gamma}^* - \frac{2}{a_o} \Delta l_s$$

where Δl_s is defined, as a function of shear strain $\bar{\gamma}^*$. The mean strain rate is given by the first derivative $\dot{\bar{\gamma}} = \partial \bar{\gamma} / \partial t$.

The mean shear strain $\bar{\sigma}_{12}$ can be calculated from the relation

$$(2.4) \quad \bar{\sigma}_{12} = [F_1(t) + F_2(t)] / 4A_s$$

where $F_1(t)$ and $F_2(t)$ are forces acting on two ends of the shear device, they can be expressed as functions of $e_i(t)$, $e_r(t)$ and $e_{ii}(t)$ using the Hook's law. Also, the mean shear strain is given in the following form

$$(2.5) \quad \sigma_{12} = \frac{1}{4} E_o \frac{A_H}{A_s} [\varepsilon_i(t) + \varepsilon_r(t) + \varepsilon_{ii}(t)]$$

where E_o is the Young's modulus and A_H is the cross section area of Hopkinson bars. It must be remembered that all those relations have been derived using the elementary wave theory of longitudinal elastic waves.

We obtain directly the hardening function $\sigma_{12}(\gamma)$ of the examined specimen in simple plane shear. Using this method, we can determine the surface $f(\sigma_{12}, \gamma, \dot{\gamma}) = 0$ if we assume that the time of transition of waves through the specimen is very small compared to the total time of loading by the first pulse. The result of multiple reflections of the loading waves in the specimen is the uniform distribution of strains and stresses in the whole gauge section.

The $\sigma_{12}(\gamma)$ curves for high strain rates are shown in Fig. 14, for the DH-36 steel sheets. In this experiment we use the projectile of the length 150 mm, strikes with the impact velocity from 10 to 12 m/s. We observe very high level of stress for small shear deformations.

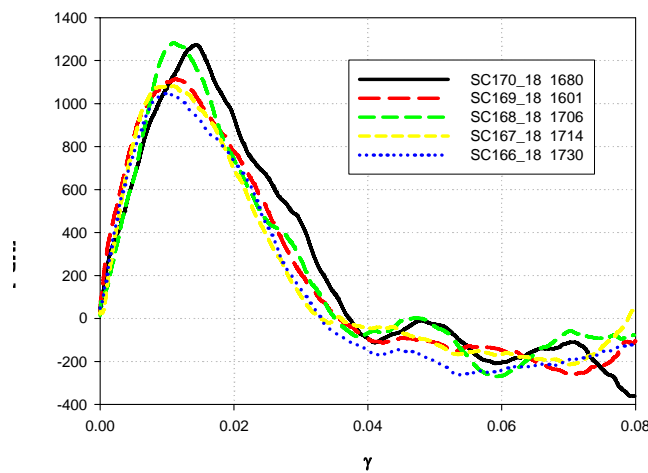


Figure 14. Shear stress $\tau = \sigma_{12}$ – shear strain γ curves obtained at high strain rates of the order of $1.7 \times 10^3 \text{ s}^{-1}$ for DH-36 steel sheets

2.3. Metallurgical observations. In the Fig. 15 microstructure in DH-36 steel before testing is shown. Average diameter of grain was a 10 μm . Using metallographic microscope observation, changes in the microstructure in the shear zones deformed to 40% after dynamic simple shear are not visible.

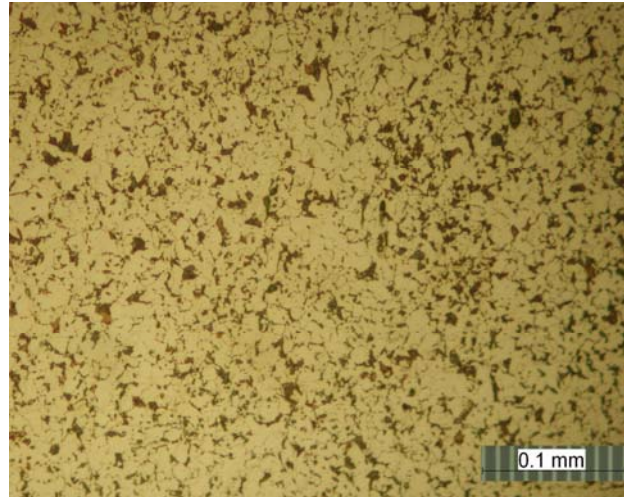


Figure 15. Microstructure in DH-36 steel before simple shear.

In the Fig. 16 we can observed that the specimen is deformed not only between the grips, in the gauge section. The part under the grips is partially deformed too. The transversal strike lines, provided from mechanical polishing of the specimen before the test, become after deformation the curves with the strike sections.

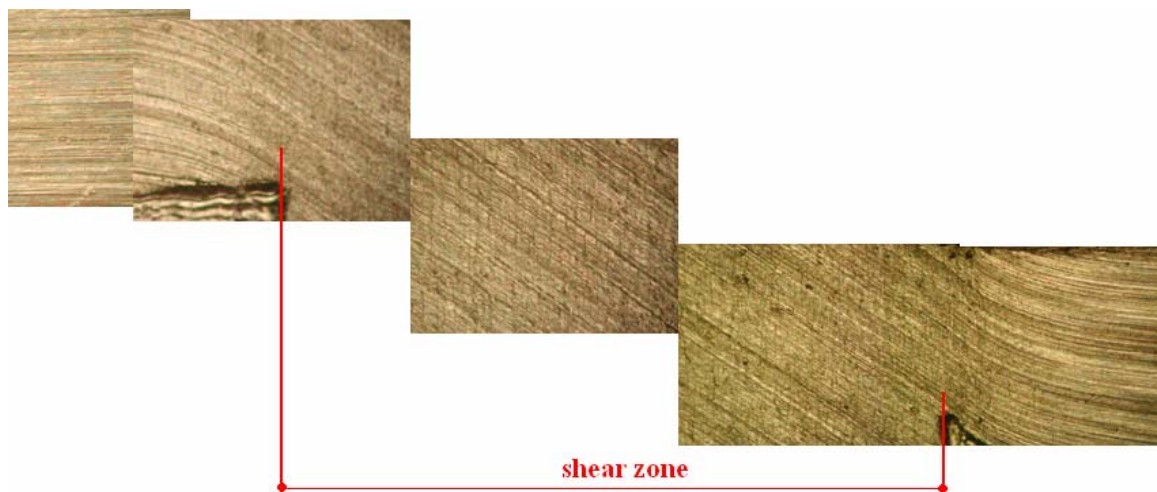


Figure 16. Displacement between external and internal grips under metallographic microscope. Length of the shear zone is equal to 3 mm.

2.4. Dynamic tests in simple shear at very high strain rates. The highest strain rate in the specimen can be obtained using only one bar of the SHPB system. We use the transmitting bar only (tube) and the shearing device is placed in front of this bar. This technique is based on the principle given by Dharan and Hauser [13]. In this new experimental technique, the flat projectile strikes directly the double shear specimen placed in the device on the front of the transmitting bar, as shown in Fig. 17. In this technique, the transmitting bar has the form of a tube. We have to register only the transmitted impulse ε_t and the velocity of the projectile. The set-up with three light beams makes it possible to determine the acceleration/deceleration of the projectile just before impact and, thus, the exact value of v_o can be determined.

The axial displacement Δl imposed on the double shear specimen by a projectile impact can be found as follows: $\Delta l(t) = \delta_l(t) - \delta_2(t)$, where $\delta_l(t)$ is the axial displacement of the internal part of the shearing device with respect to the external part, $\delta_2(t)$ is the displacement of the Hopkinson tube, given by

$$(2.6) \quad \delta_1(t) = v_o t \quad \text{and} \quad \delta_2(t) = c_o \int_0^t \varepsilon_t(\tau) d\tau$$

where v_o is the impact velocity of the projectile, c_o is the elastic wave speed in the Hopkinson tube, and $\varepsilon_t(t)$ is the transmitted signal in the Hopkinson tube, measured by the strain gauge T_1 . The axial displacement $\delta_l(t)$ of the central part of the double shear specimen is measured as a function of time by an optical extensometer, acting as a contact-less displacement gauge.

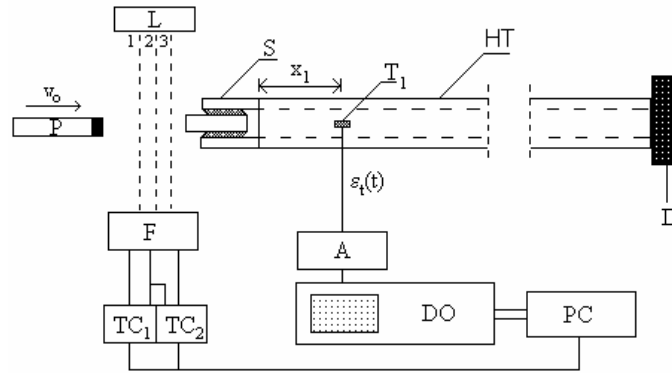


Figure 17. Configuration of experimental set-up for direct impact. *S* – shear device with a double shear specimen, *HT* - Hopkinson tube (transmitter bar), *P* - projectile, *D* - damper, *L* - laser, *F* - photodiodes, *TC* - time counter, *T₁* - strain gauge, *A* - amplifier, *DO* - digital oscilloscope, *PC* - computer

The mean shear strain and the mean strain rate can be found as

$$(2.7) \quad \bar{\gamma}(t) = \frac{1}{a_o} \left[v_o t - c_o \int_0^t \varepsilon_t(\tau) d\tau \right], \quad \dot{\bar{\gamma}}(t) = \frac{1}{a_o} [v_o - c_o \varepsilon_t(t)]$$

The shear stress can be expressed as

$$(2.8) \quad \bar{\sigma}_{12}(t) = \frac{S_T}{2S_E} E_o \varepsilon_t(t),$$

where E_o is the Young modulus of the tube, $S_T = \pi(d_2^2 - d_1^2)/4$, d_1 and d_2 are the internal and external diameters of the tube, respectively. Thus, the shear stress in the double-shear specimen is proportional to the current signal of the transmitted longitudinal wave ε_t . A typical oscillogram obtained from the direct impact technique for DH-36 sheet metals is shown in Fig. 18. Because of a high strain rate of the order $\dot{\gamma} = 6.2 \cdot 10^3 \text{ s}^{-1}$, vibrations in the shear device are inevitable.

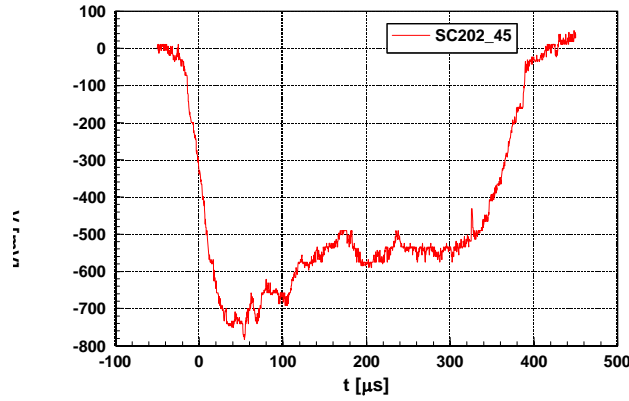


Figure 18. Oscillogram from the direct impact test at velocity $v_o = 20 \text{ m/s}$

Results of experimental investigations of DH-36 steel in the case of dynamic simple shear at very high strain rates from $5.2 \cdot 10^3 \text{ s}^{-1}$ to $6.2 \cdot 10^3 \text{ s}^{-1}$ are presented in the Fig. 19. We can compare shear stress - shear strain curves obtained in the dynamic test at very high strain rates. From this picture we are able to determine the shear strain corresponding to ductile fracture from the condition $d\tau/d\gamma = 0$.

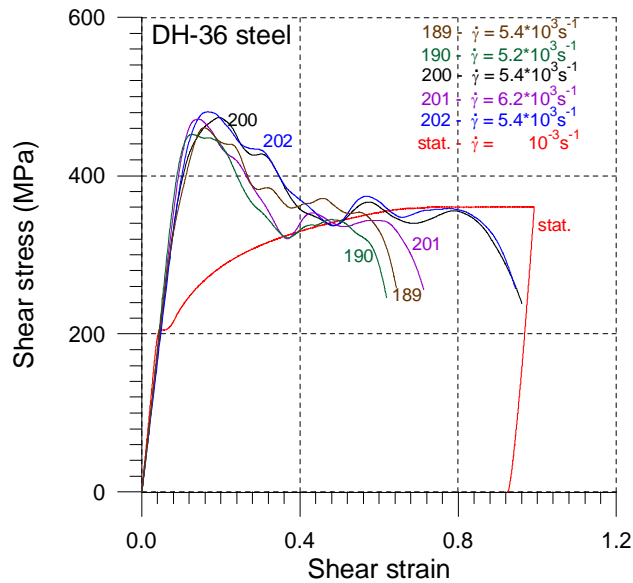


Figure 19. Stress-strain relation obtained during dynamic simple shear of DH-36 steel (direct impact); 189 ÷ 202 – tests numbers

Figure 20 shown the comparison of the shear stress – shear strain curves in case of the dynamic loading (direct impact test) at the strain rate $6.3 \cdot 10^3 \text{ s}^{-1}$ with the quasi-static curves.

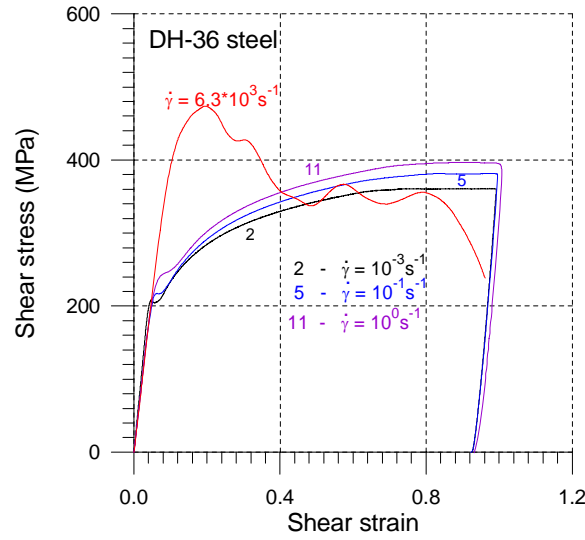


Figure 20. Comparison of stress-strain characteristics obtained during quasistatic and dynamic tests

In the case of quasi-static simple shear of DH-36 steel the maximum values of shear stresses are situated on the level of 400 MPa – cf. Figs 7 to 9. The comparison of maximum shear stress in the quasi-static and dynamic tests at high strain rate higher than 10^3 s^{-1} is shown on the Fig. 21.

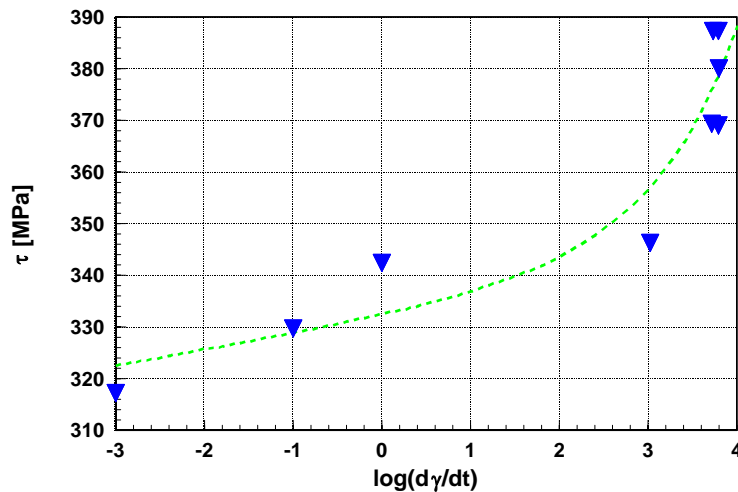


Figure 21. Shear stress τ versus logarithmic shear strain rate $d\gamma/dt$

In the Table 2 all experimental results in dynamic test (in the case of SHB - Split Hopkinson Bar technique and in the case of DI – direct impact of the projectile into the shear sample) are collected.

Remarks to the Table 2.

scale	Generally	shear bands
0	lack	absent
1	Weak	mat at the specimen surface
2	Strong	sharp line of the shear bands on the specimen surface

Impactor	Length
LP	L=300 mm
MP	L=150

Test	
DI	direct impact
SHB	Shear in Split Hopkinson Pressure Bars

Table 2. Results of dynamic tests in simple shear

Test number	Specimen number	Impactor	Test	a_0 [mm]	v_p [m/s]	E_{kp} [J]	δu [mm]	γ_{end}	dy/dt_{max}	τ_{max} [MPa]	τ_{avg} [MPa]	stress concentration at the end of shear zone	breaking at the end of the shear zone	shear band	macroscopic shear band	partial cracking
155	21	MP	SHB	0.650	5.45	4.4	0.99	33%				1	1	1	0	0
160	16	MP	SHB	0.640		0.0	0.38	13%				1	1	1	0	0
161	23	MP	SHB	0.647	6.94	7.2	0.28	9%				1	1	0	0	0
162	23	MP	SHB		3.03	1.4		0%	957	439	367	1	1	0	0	0
163	24	MP	SHB	0.624	10.65	17.0	0.64	21%	1743	648	644	1	1	1	0	0
164	18	MP	SHB	0.635	10.50	16.5	0.67	22%	1522			1	1	1	0	0
165	19	MP	SHB	0.640	10.04	15.1	0.73	24%	1695			1	1	1	0	0
166	22	MP	SHB	0.654			1.38	46%	2218			1	1	2	0	0
167	25	MP	SHB	0.656			1.26	42%	2157			1	1	1	0	0
168	26	MP	SHB	0.652	12.88	24.9	0.88	29%				1	1	1	0	0
169	27	MP	SHB	0.640	11.98	21.5	1.13	38%	2026			1	1	1	0	0
170	28	MP	SHB	0.648	3.97	2.4	1.21	40%	2097			1	1	1	0	0
171	29	MP	SHB	0.650	13.96	29.2	1.52	51%	2291							
172	30	MP	SHB	0.651	14.63	32.1	1.59	53%	2615			1	1	1	0	0
173	31	MP	SHB	0.642	13.88	28.9	1.3	43%	2306			1	1	1	0	0
174	32	MP	SHB	0.651			0.69	23%	1747			1	1	1	0	0
177	33	LP	SHB	0.656	7.96	19.0	0.99	33%	1183			1	1	1	0	0
178	34	LP	SHB	0.655	8.03	19.4	0.98	33%				1	1	1	0	0
179	35	LP	SHB	0.650	7.57	17.2	0.92	31%	1287			1	1	1	0	0
189	17	MP	DI	0.635	16.99	43.3	3.39	113%	5411	393	387	2	2	2	0	0
190	36	MP	DI	0.647	16.37	40.2	3.7	123%	5226	414	369	1	2	2	0	0
200	37	MP	DI	0.648	19.69	58.2	4.86	162%	6302	458	380	2	2	2	1	1
201	39	MP	DI	0.650	19.32	56.0		0%	6210	439	369	2	2	2	1	1
202	40	MP	DI	0.652	19.67	58.1	4.67	156%	6208	408	387	2	2	2	1	1
203	38	MP	DI	0.630	3.77	2.1	3.04	101%	1058	346	346	2	2	2	1	1

Classification trees are used to predict membership of cases in the classes of categorical dependent variable. To calculating we have used application the STATISTICA version 6. All results of dynamical experiments are gathered in Table 2. As dependent variable the partial cracking was chosen. For physical reason we have get a set of independent variables listened in the Table 3.

Table 3. Importance of the independent variables

			Variable rank	Importance
kinetic energy of impactor	E_{kp} [J]	E_{kp} [J]	82	0.817353
deformation	γ_{end}	g_{end}	63	0.626555
deformation rate	$d\gamma/dt$ max	dg/dt max	100	1.000000
maximal shear stress	τ_{max} [MPa]	t_{max} [MPa]	100	1.000000
average shear stress	τ_{avg} [MPa]	t_{avg} [MPa]	64	0.642952
			100 - the best	

Variable rank is calculated by algorithm of the classification using correlation between all variables. The classification algorithm was applied to $N=23$ samples. According this classification the most important, strong correlated, are: deformation rate, maximum shear stress and weaker kinetic energy of projectile, see Table 3 and Fig. 22. In the Fig. 23 levels of the classification for both the most important variables are presented, $d\gamma/dt=5800$ 1/s and $\tau_{max}=369.5$ MPa. Algorithm of classification is stopped on the second level of the classification tree when the split error of the samples is less then 0.05.

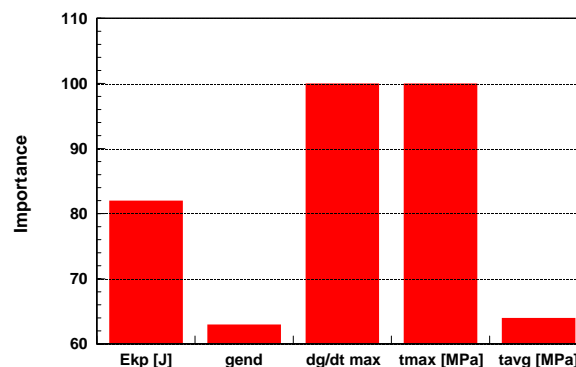


Figure 22. Importance plot. Dependence variable: partial cracking

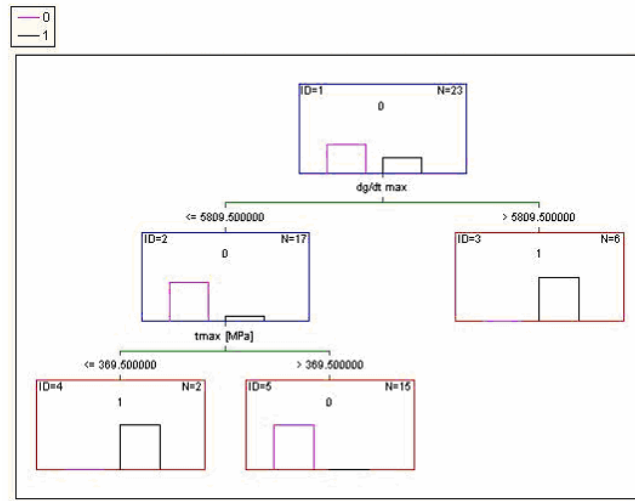


Figure 23. Tree: graph for variable partial cracking. Number of non-terminal nodes 2, Number of terminal nodes 3

2.5. Comparison of simple shear test with compression test. To understand the mechanical response of DH-36 steel, uniaxial compression tests are performed on small cylindrical specimens, using an Instron testing machine. True strains exceeding 40% are achieved in these tests in the quasistatic conditions of loadings, with strain rates of the order of $6 \cdot 10^{-2} \text{ s}^{-1}$. All tests are carried out on a DH-36 baseplate. All samples used in the compression test have 8 mm nominal diameter and 8 mm high. To reduce the end friction on the samples during deformation, the sample ends are polished and greased. The stress-strain relation in the compression test is presented in the Fig. 24.

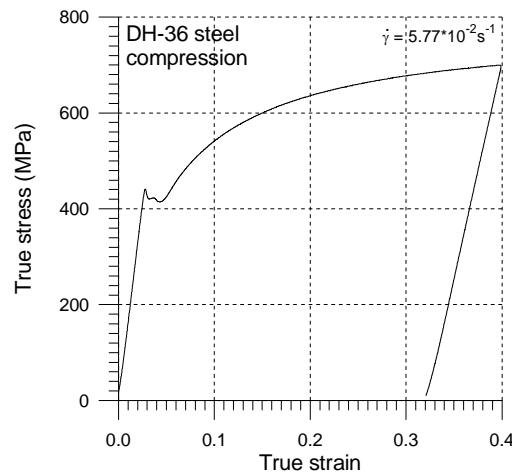


Figure 24. Quasi-static compression test of the DH-36 steel, strain rate $5.77 \cdot 10^{-2} \text{ s}^{-1}$

Comparison of the result obtained in the simple shear test and the compression test for DH-36 steel at low strain rate $5.77 \cdot 10^{-2} \text{ s}^{-1}$ is shown in Fig. 25. We assume the Huber-Mises-Hencky yield criterion: $\gamma = \varepsilon_{11} / \sqrt{3}$ and $\sigma_{12} = \sqrt{3}\sigma_{11}$.

In fact, the influence of stress components σ_{11} and σ_{22} must be taken into account. The stress intensity is defined as: $\sigma_i = [\sigma_{11}^2 + \sigma_{22}^2 + 3\sigma_{21}^2 - \sigma_{11}\sigma_{22}]^{1/2}$.

We can observe that the hardening of the material is similar for different values of the strain rate (the same effect is observed in the case of the Tresca yield condition). In the case of Huber-Mises-Hencky (HMH) yield condition, an important difference in stress increment is observed. The existence of a difference between simple shear tests and tensile tests after application of the HMH criterion was also observed by various authors. They explain this difference by the different systems of slip activated according to the type of loading and interaction of displacements at long and short distance. Also, for the metal like the DH-36 steel, the HMH yield criterion is not the best.

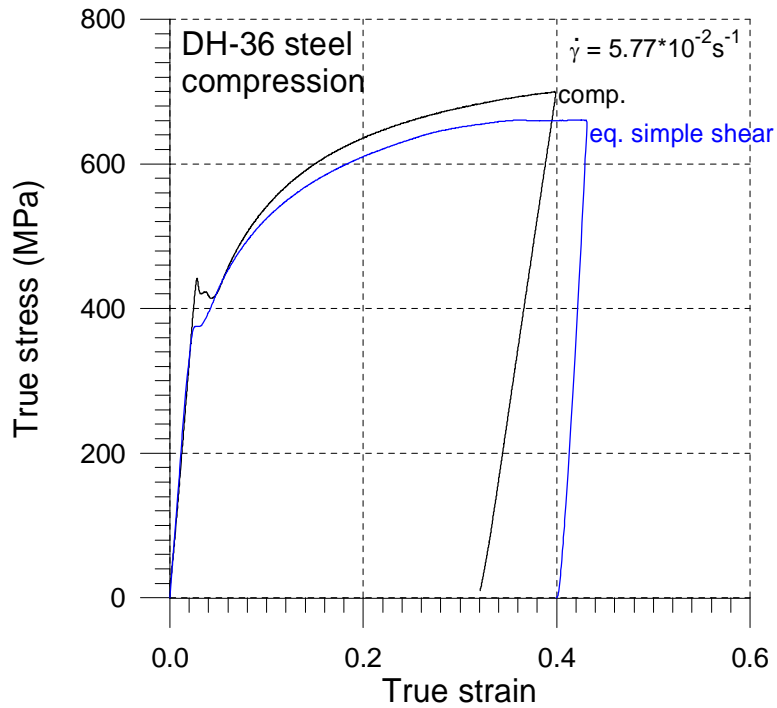


Figure 25. Comparison of the shear and tension test at strain rate $5.77 \cdot 10^{-2} \text{ s}^{-1}$

3. Constitutive model in application for finite element simulation of dynamic experiments and construction of the dynamic fracture locus

The simple shear in the direction \mathbf{e}_1 of the coordinate system $(\mathbf{e}_1, \mathbf{e}_1)$ is defined by the relations

$$u_1 = \gamma(t) x_2, \quad u_2 = u_3 = 0,$$

$$v_1 = \dot{\gamma} x_2, \quad v_2 = v_3 = 0,$$

where $\gamma = \tan \varphi$ (cf. Fig. 26) and $\dot{\gamma}$ are the plastic shear strain and shear strain rate, respectively.

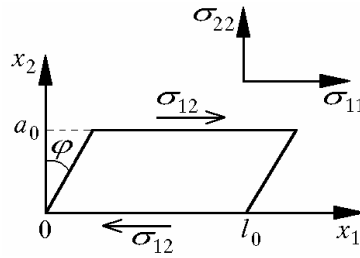


Figure 26. Scheme of simple shear

From the velocity field \mathbf{v} , the velocity gradient \mathbf{V} , the rate of deformation \mathbf{D} and the material spin $\mathbf{\omega}$ can be determined in the system $(\mathbf{e}_1, \mathbf{e}_1)$ as

$$\mathbf{V} = \frac{\dot{\gamma}}{2} \begin{pmatrix} 0 & 1 \\ 0 & 0 \end{pmatrix} \quad \mathbf{D} = \frac{\dot{\gamma}}{2} \begin{pmatrix} 0 & 1 \\ 1 & 0 \end{pmatrix} \quad \mathbf{\omega} = \frac{\dot{\gamma}}{2} \begin{pmatrix} 0 & 1 \\ -1 & 0 \end{pmatrix}.$$

The Cauchy stress tensor $\boldsymbol{\sigma}$ has the non-zero components

$$\boldsymbol{\sigma} = \begin{pmatrix} \sigma_{11} & \sigma_{12} \\ \sigma_{21} & \sigma_{22} \end{pmatrix}$$

The program of finite element method was used to the numerical simulations of the formulated problem of quasi-static and dynamic simple shear of thin sheets. We assume the initial and boundary conditions similar to those used in the experiment.

In the case of quasi-static loading, the boundary conditions have the following form:

in fixed ends of specimen (under grips) – cf. Figure 26:

$$u_1(x_1, x_2, t) \Big|_{x_2=0} = u_2(x_1, x_2, t) \Big|_{x_2=0} = 0,$$

$$v_1(x_1, x_2, t) \Big|_{x_2=a_o} = v_o \quad \text{and} \quad u_2(x_1, x_2, t) \Big|_{x_2=a_o} = 0.$$

where v_o is the velocity of the testing machine in traction. In this case, the sliding of material under the grips is neglected.

At the free ends of the specimen (for $x_1 = 0$ and $x_1 = l_o$) we have:

$$\sigma_{12}(x_1, x_2, t) \Big|_{\substack{x_1=0 \\ x_1=l_o}} = \sigma_{11}(x_1, x_2, t) \Big|_{\substack{x_1=0 \\ x_1=l_o}} = -\sigma_{22}(x_1, x_2, t) \Big|_{\substack{x_1=0 \\ x_1=l_o}} = 0.$$

In the case of dynamic deformations, these conditions must be replaced by conditions of balance of forces in the contact between the specimen and the measuring bars. We should remember that the shear device and bars of SHPB system have identical mechanical impedances.

In the analysis, we must take into account that the loading of the specimen is not instantaneous. The loading compression wave must take some time to transmit from one end of the device to the other. In the first step a simplifying assumption can be introduced, and the process of waves propagation in the specimen can be neglected. However, it is worthwhile to notice that, in our tests, a very accurate equilibrium is obtained regarding the forces on two sides of the shear device, in the time period $50 \mu s < t < 500 \mu s$. The force is taken to be equal to the mean value of input and output force.

The amplitude of loading is determined from the dynamic experiment. We assume that in the contact between the specimen and measuring bars, the force is constant in time and equal to F_{max} . The boundary conditions take the form:

$$\sigma_{12}(x_1, x_2, t) \Big|_{x_2=0} = -F_{max} / S_E \quad \text{and} \quad u_2(x_1, x_2, t) \Big|_{\substack{x_2=0 \\ x_2=a_o}} = 0.$$

We assume the homogeneous zero initial conditions.

In the finite element method the rectangular mesh is introduced. Deformation of the mesh in time is determined. At the same time, the components of the stress tensor σ_{12} and $\sigma_{22} = -\sigma_{11}$, the stress intensity $\sigma_i = (3/2 s_{ij} s_{ij})^{1/2}$ and the equivalent strain $e_i = (2/3 \varepsilon_{ij}^p \varepsilon_{ij}^p)^{1/2}$ are determined.

3.1. Constitutive description of inelastic deformation in application for the study of strain rate effect on ductile fracture. We assume that a multiscale approach, which was proposed in relation to plastic flow of metals accounting for shear banding, in refs [17-19], can be extended to describe plastic deformation of DH-36 steel. This is justified by the results of microstructural observations presented in [15], where: “*shear bands are seen to have formed at an angle 45° to the loading direction (Figs. 17 and 18), and within the shear bands, the grains are seen to have been extended in the shear band direction*”, p. 1034 in [15].

Among many possible realizations of shear banding processes one can single out the group of processes characterizing, at least approximately or for sufficiently long deformation paths, with the same contribution of two systems of shear bands, i.e. $f_{SB}^{(1)} = f_{SB}^{(2)}$, where f_{SB}^i is the shear banding function describing the contribution of the shear banding system $i=1$ and $i=2$, respectively, in the total plastic shear strain rate [19]. On the other hand, the non-symmetric activation of shear bands can be induced by a sufficiently large change of loading direction or rotation of the principal axes of the stress tensor in the inhomogeneous deformation process caused by boundary conditions. Therefore, we postulated in [20] that:

$$(3.1) \quad \Delta f_{SB} = 0 \text{ for } \delta \in [0, \delta_c] \text{ and } \Delta f_{SB} = A(\delta) \text{ for } \delta \in \left(\delta_c, \frac{\pi}{2}\right], \quad \tau' : \mu_F = \left| \tau' \right| \cos \delta.$$

The function $A(\delta)$ being a measure of the mentioned asymmetry of shear banding should be identified from numerical simulations of the experiment accounting for the change of loading direction.

Because of the above assumptions, the plastic flow laws take the form:

- For the case in which the loading direction described by the objective rate of stress $\overset{\circ}{\tau}$ is pointing at partially active range, i.e. for $\delta \in \left(\delta_c, \frac{\pi}{2}\right]$

$$(3.2) \quad \mathbf{D}^p = \frac{\tau' : \mu_F}{2h(1-f_{SB})} \mu_F + \frac{\tau' : \mu_F}{2h(1-f_{SB})} \frac{A(\delta) \tan 2\beta}{\left\| \tau' \right\| \sin \delta'} \left[\overset{\circ}{\tau} - \left(\tau' : \mu_F \right) \mu_F \right],$$

- For the case in which the objective rate of stress $\overset{\circ}{\boldsymbol{\tau}}$ is pointing at fully active range, i.e. for $\delta \in [0, \delta_c]$:

$$(3.3) \quad \mathbf{D}^p = \frac{\overset{\circ}{\boldsymbol{\tau}} : \boldsymbol{\mu}_F}{2h(1 - f_{SB})} \boldsymbol{\mu}_F, \quad \boldsymbol{\mu}_F = \frac{1}{\sqrt{2}k} \boldsymbol{\tau}'.$$

The Huber-Mises yield condition is assumed: $J_2 = k^2$, where $J_2 = \frac{1}{2} \boldsymbol{\tau}' : \boldsymbol{\tau}'$ and the symbol k denotes the yield limit obtained in a shear test. The above-mentioned assumptions leading to the simplified formula (3.3) find confirmation in experimental observations for metallic materials, which show that the spatial pattern of micro-shear bands does not change for loading conditions that deviate within limits from the proportional loading path, i.e. the load increments are confined to a certain cone (fully active range) the angle of which can be determined experimentally, [19]. The specification of these equations and the identification of the shear banding contribution function f_{SB} are discussed in [20].

If the dependence on strain rate comes into play, the viscoplasticity flow law can be applied [21]:

$$(3.4) \quad \mathbf{D}^p = \dot{\gamma}^{vp} \boldsymbol{\mu}_F, \quad \boldsymbol{\mu}_F = \frac{1}{\sqrt{2}k} \boldsymbol{\tau}',$$

where $\dot{\gamma}^{vp}$ is the viscoplastic shear strain rate determined in the following way for the exponential overstress function

$$(3.5) \quad \dot{\gamma}^{vp} = \dot{\gamma}_0 \exp \left[\frac{J_2}{(1 - f_{SB}) [A + B(\dot{\gamma}^{vp})^n]} - I \right].$$

Where the power-like strain hardening law is assumed.

According to the analysis in [20], the shear banding function takes the form:

$$(3.6) \quad f_{SB} = \frac{f_{SB_0}}{1 + \exp(a - b|\dot{\gamma}^{vp}|)}.$$

The yield condition $J_2 = k_d$ is obtained by inverting (3.5)

$$(3.7) \quad k_d = (1 - f_{SB}) \left[A + B(\gamma^{vp})^n \right] \left[1 + C \ln \dot{\gamma}^* \right].$$

where $\dot{\gamma}^* = \frac{\dot{\gamma}^{vp}}{\dot{\gamma}_0}$, $\dot{\gamma}_0 = 2 \times 10^{10} \text{ s}^{-1}$.

The formula (3.7) shows that Perzyna model with the exponential overstress function and the assumed strain hardening law is equivalent to the Johnson-Cook model considered in [15].

In our case the results presented in [15] can be used, where the Johnson-Cook model was identified for DH-36 steel. If the effects of shear bands and temperature are neglected we have

$$(3.8) \quad k_d = \frac{\sqrt{3}}{3} \left(A + B(\gamma^{vp})^n \right) \left(1 + C \ln \dot{\gamma}^* \right),$$

where $A = 1020 \text{ MPa}$, $B = 1530$, $C = 0.015$, $n = 0.4$ and $\dot{\gamma}^* = \frac{\dot{\gamma}^{vp}}{\dot{\gamma}_0}$, $\dot{\gamma}_0 = 2 \times 10^{10} \text{ s}^{-1}$.

3.2. Conclusions

Application of the general scheme of calibration of fracture model proposed e.g. by Y. Bao, Y.-W. Lee and T. Wierzbicki [16] to the investigated experimentally material (DH-36 steel) consists of the following steps:

1. Experimental determination of stress-strain characteristics of DH3-steel under quasi-static and dynamic loading conditions, e.g. in tension or compression tests.
2. Identification of viscoplasticity model accounting for shear banding.
3. Measurements of force-displacement response of simple shear test.
4. Development of finite element model of a specimen and numerical simulation of the loading process.

5. Calculation of the evolution of equivalent strain and the stress triaxiality at the critical point (detected during the test with use of thermovision camera).
6. Determination of the equivalent strain to fracture from the comparison between the tests and numerical simulations.

An example of the force-displacement response of simple shear test performed with use of DH-366 steel samples is shown in Fig. 27. The development of finite element model of a specimen used in the simple shear test is depicted in Fig. 28. This makes a basis for the numerical simulation of the loading processes at different strain rates and performing of further steps of the calibration procedure. Realization of these steps should contribute in future to the construction of the limiting failure curve (fracture locus) for different strain rates.

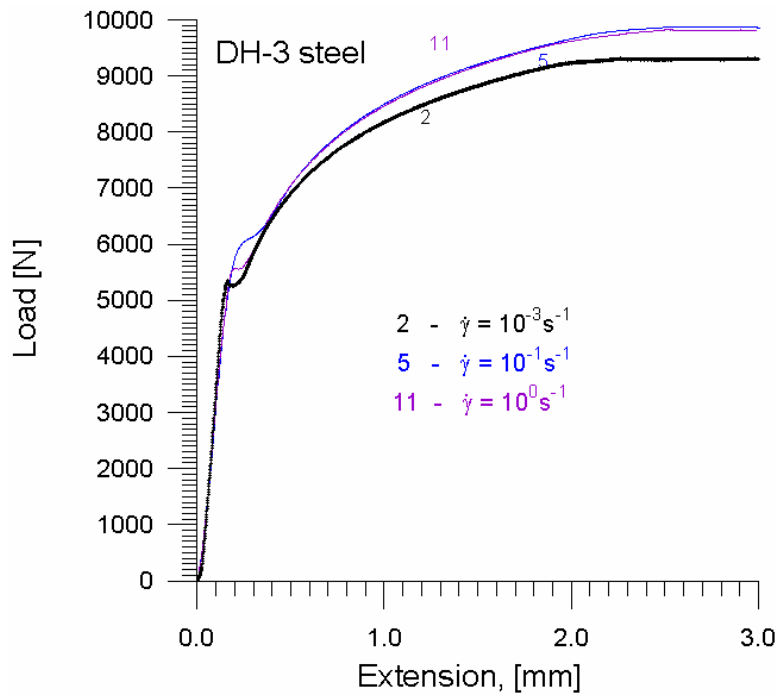


Figure 27. Load – extension curves obtained in simple shear tests for different strain rates, DH-36 steel.

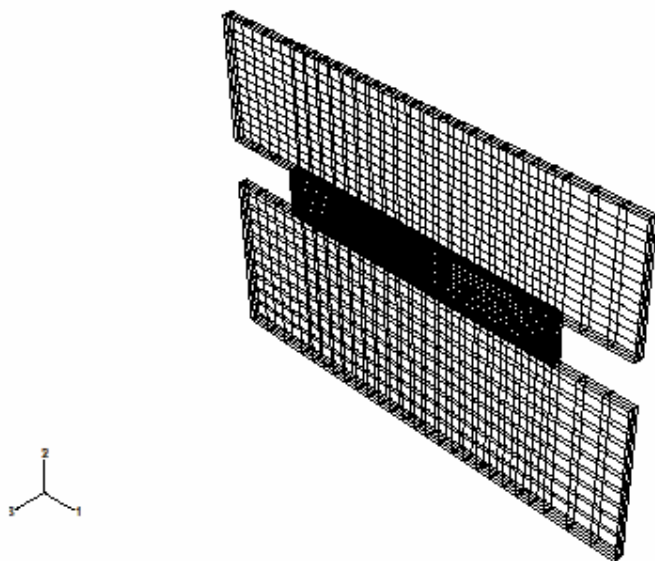


Figure 28. Assumed shape of the specimen and the initial mesh.

4. Annex I – PP - presentation – seminar at MIT

Prof. R. B. Pęcherski took part in the Workshop on Computational Fracture Mechanics and ICL Review Meeting, MIT, October 13-14, 2005 and presented the lecture prepared jointly with Prof. W.K. Nowacki on: “A New Experimental Technique for Studying Strain Rate Effects on Fracture”. During the lecture the potential in the field of experimental and theoretical investigations of the team at the Institute of Fundamental Technological Research in the joint research project was presented. The main subject of the discussion after the presentation was related with the simple shear test at different strain rates and the possibilities of detecting the region of fracture initiation.

5. Annex II - Micromechanics of localized fracture phenomena in inelastic solids – by Z. Nowak, P. Perzyna and R.B. Pęcherski

References

1. Gary, G., Nowacki, W.K., 1994, Essai de Cisaillement Plan Dynamique Appliquée a des Tôles Minces, *Journal de Physique IV*, **C8**, 65-70.
2. Nguyen, H.V., Nowacki, W.K., 1998, Localization of thermo-elastoplastic deformations in the case of simple shear, *Journal of Thermal Stresses*, 3-4, **21**, 341-357.
3. G'Sell. C., Boni. S., Shrivastava, S., 1983, Application of the Plane Shear Test for Determination of the Plastic Behaviour of Solids Polymers at Large Strain, *J. of Mat. Sciences* **18**, 903-918.
4. Tourabi, A., Wack, B., Guélin, P., Favier, D., Pegon, P., Nowacki, W.K., 1993, Remarks on an experimental plane shear test and on an anisotropic elastic-plastic theory, *Technical Report, SMIRT, 1993, Stuttgart, August 15-20, Elsevier Sci. Publ.*
5. Rauch, E.F., G'Sell C., 1998, Flow localization induced by a change in strain path in mild steel, *Material Sci. and Eng.*, (A111), 71.
6. Wack, B., Tourabi, A., 1993, Cyclic simple shear of metallic sheets (applications to aluminium-lithium alloy), *J. Mater. Sci.*, 4735-4743.
7. Manach, P.Y., Favier, D., 1997, Shear and tensile thermomechanical behavior of near equiatomic NiTi alloy, *Materials Scie. and Engineering*, A 122, 45-57.
8. Yoshida, K., Myauchi, K., 1978, Experimental Studies of Mechanical Behaviour as Related to Sheet Metal Forming, in *Mechanics Sheet Metal Forming*, Plenum Press, New York, 19-49.
9. Marchand, A., Duffy, J., 1988, An experimental study of the formation process of adiabatic shear bands in structural steel, *J. Mech. Phys. Solids.*, **36**, 3, 251-283.
10. Nowacki W.K., 2001, Dynamic simple shear of sheets at high strain rates, in *Impact Engineering and Application*, Proc. of 4th International Symposium on Impact Engineering, Elsevier, 83-90.
11. Kelvin L., 1853, *On the thermoelastic and thermo-magnetic properties of matter*, Trans. Roy. Soc. Edinb., **20**, 161, 57-77.
12. Rusinek A., Gadaj S.P., Nowacki W.K., Klepaczko J.R., 2002, *Simulation of heat exchange during simple shear of sheet steel*; Journal of Theoretical and Applied Mechanics, **40**, 2, 317-337

13. Dharan, H.C.K., Hauser, F.E., 1970, Determination of stress-strain characteristics at very high strain rates, *Exp. Mech.*, **10**, 370-376.
14. Gadaj, S.P., Nowacki, W.K., Pieczyska, E., 1996, Changes of temperature during the simple shear test of stainless steel, *Arch. of Mechanics*, **48**, 4, 779-788.
15. S. Nemat-Nasser, W.-G. Guo, Thermomechanical response of DH-36 structural steel over a wide range of strain rates and temperatures, *Mech. Materials*, 35, 1023-1047, 2003.
16. Bao Y., Lee Y. W. and Wierzbicki T., Evaluation of the Wilkins (and other) Fracture Models, Impact & Crashworthiness Laboratory, MIT, Report No:120, May 2004.
17. Pęcherski R.B., Macroscopic measure of the rate of deformation produced by micro-shear banding, *Arch. Mech.*, 49, 385-401, 1997.
18. Pęcherski R.B., Macroscopic effects of micro-shear banding in plasticity of metals, *Acta Mechanica*, 131, 203-224, 1998.
19. Pęcherski R.B., Korbel K., Plastic strain in metals by shear banding. I. Constitutive description for simulation of metal shaping operations *Archives of Mechanics*, 54, 603-620, 2002.
20. Nowak Z., Pęcherski R.B., Plastic strain in metals by shear banding. II. Numerical identification and verification of plastic flow law accounting for shear banding, *Archives of Mechanics*, 54, 621-634, 2002.
21. Perzyna P., Fundamental problems in viscoplasticity, *Advances in Mechanics*, 9, 243-377, 1966.

A New Experimental Technique for Studying Strain Rate Effect on Fracture

W.K. Nowacki & R.B. Pecherski

1. Our tradition in energy-based approach to fracture research
2. Experiment: dynamic simple shear test and tension test of sheets at high strain rates
3. Measurement of temperature during dynamic simple shear
4. Numerical analysis and comparison with experimental results
5. Comparison of simple shear test with tension test
6. Conclusions

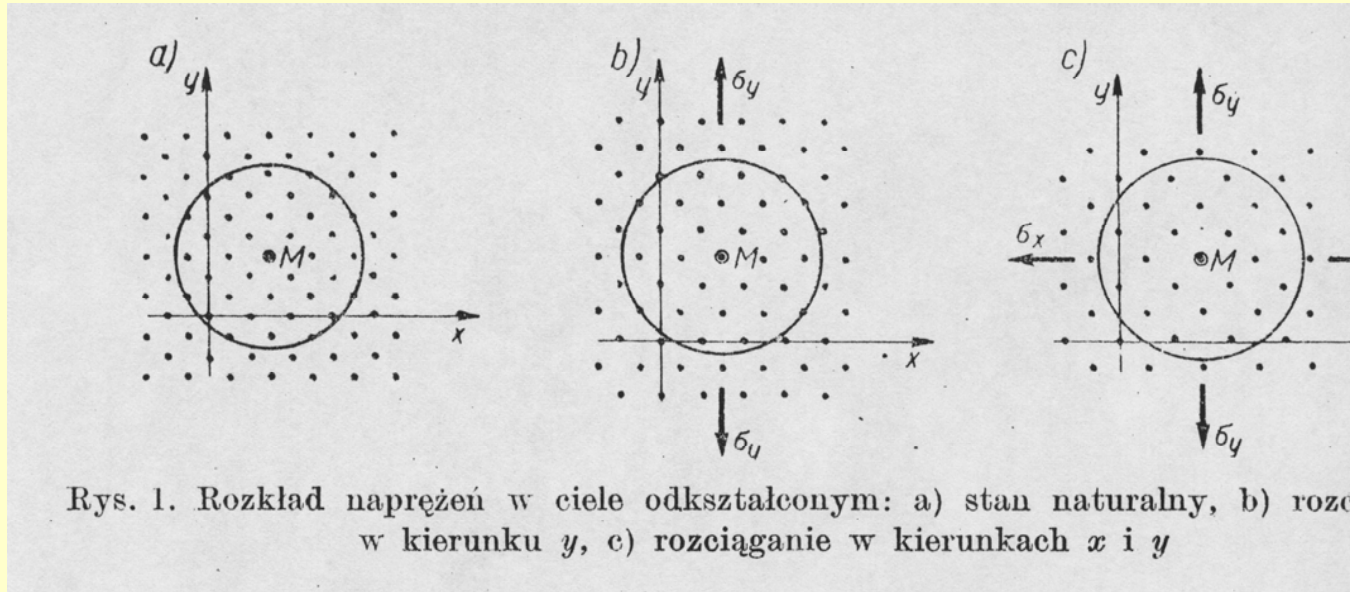
Our tradition in fracture research

Phenomenological criteria of strength (material effort):

- energy based approach for isotropic solids (M.T. HUBER [1904])
- Volume-distortional energy hypothesis accounting for the effects of triaxial states - W.T. BURZYNSKI [1928],
- application of energy based approach for orthotropic solids - W.T. BURZYNSKI [1928],
- Energy-based approach for solids with arbitrary symmetry J. RYCHLEWSKI [1984],
- Energy-based approach applied for cellular solids and foams of different symmetry R.B. PECHERSKI et al. [2003-2005].

M. T. HUBER (1872-1950)

Czasopismo Techniczne, Lwów (Lemberg) [1904]



"Specific Strain Work as a Measure of Material Effort - A Contribution to Foundations of the Theory of Material Strength" – ARCHIVES OF MECHANICS, **56**, No. 3, 173-190, 2004 (English translation on the centenary of the first Polish edition).

The specific work of strain is equal to the work performed by intermolecular forces acting between molecules Since the work of intermolecular forces is the greater the larger are the relative displacements of the molecules in strain a very probable hypothesis suggests itself that:

Material effort is measured by specific work of strain.

Then, if in a certain point of the body work of strain goes beyond a determined value depending on the material, a permanent separation of molecules of the body, that is its fracture, must occur.

Huber-Mises criterion

Linear elasticity - Hooke's material:
strain work = stored elastic energy



$$\Phi = \Phi_v + \Phi_f$$

$$\frac{1}{\sqrt{2}} \sqrt{(\sigma_1 - \sigma_2)^2 + (\sigma_2 - \sigma_3)^2 + (\sigma_1 - \sigma_3)^2} = R_e$$

R.von Mises (1913) – quadratic
approximation of Tresca criterion.



Richard von MISES (1883-1953)

W. T. BURZYŃSKI (1900-1970)



„Study on Material Effort Hypotheses”,
Lwów 1928.

„Ueber die Anstrengungshypothesen”,
Schweizerische Bauzeitung, **94**, 259-162, 1929.

$$\Phi_f + \eta \Phi_v = \Phi_{gr} = const, \quad 0 \leq \eta \leq 1$$

$$\frac{3}{4G} \omega_2^2 + \eta \frac{3}{4K} \omega_1^2 = const$$

$$\omega_1 = \frac{1}{3} (\sigma_1 + \sigma_2 + \sigma_3)$$

$$\omega_2 = \frac{1}{3} \sqrt{(\sigma_1 - \sigma_2)^2 + (\sigma_2 - \sigma_3)^2 + (\sigma_1 - \sigma_3)^2}$$

W.T. Burzynski [1928] - R. Hill [1949]

$$\frac{1}{3} \left[N^* (\sigma_{11} - \sigma_{22})^2 + L^* (\sigma_{22} - \sigma_{33})^2 + M^* (\sigma_{33} - \sigma_{11})^2 \right] + 2(P^* \sigma_{23}^2 + Q^* \sigma_{13}^2 + R^* \sigma_{12}^2) = \Phi_{cr},$$

$$\frac{F (\sigma_{22} - \sigma_{33})^2 + G (\sigma_{33} - \sigma_{11})^2 + H (\sigma_{11} - \sigma_{22})^2 + 2L \sigma_{23}^2 + 2M \sigma_{13}^2 + 2N \sigma_{12}^2}{3\Phi_{cr}} = 1,$$

$$F = \frac{L^*}{3\Phi_{cr}}$$

$$L = \frac{P^*}{\Phi_{cr}}$$

$$G = \frac{M^*}{3\Phi_{cr}}$$

$$M = \frac{Q^*}{\Phi_{cr}}$$

$$H = \frac{N^*}{3\Phi_{cr}}$$

$$N = \frac{R^*}{\Phi_{cr}}.$$

Energy based approach for orthotropic solids – W. Burzynski [1928]

$$\Phi = \Phi_v + \Phi_f$$

$$\Phi_v(\sigma) = \frac{1}{2} B^* (\sigma_{11} + \sigma_{22} + \sigma_{33})^2$$

$$\begin{aligned} \Phi_f(\sigma) = & \frac{1}{3} [N^* (\sigma_{11} - \sigma_{22})^2 + L^* (\sigma_{22} - \sigma_{33})^2 + M^* (\sigma_{33} - \sigma_{11})^2] \\ & + 2(P^* \sigma_{23}^2 + Q^* \sigma_{13}^2 + R^* \sigma_{12}^2), \end{aligned}$$

$$B^* = C_{11} + C_{22} + C_{33},$$

$$L^* = \frac{3}{2} (B^* - C_{33}), \quad 4P^* = C_{44} + 2C_{45} \frac{C_{24}}{C_{15}}$$

$$M^* = \frac{3}{2} (B^* - C_{32}), \quad 4Q^* = C_{55} + 2C_{56} \frac{C_{35}}{C_{26}}$$

$$N^* = \frac{3}{2} (B^* - C_{12}), \quad 4R^* = C_{66} + 2C_{64} \frac{C_{16}}{C_{34}}.$$

M. Janus-Michalska & R.B. Pecherski

Technische Mechanik, 23, 2003.

Criterion for metal foams:

$$\frac{1}{2K} \frac{\sigma^2}{\Phi_{CR1}} + \frac{1}{4G} \frac{\underline{S} \cdot \underline{S}}{\Phi_{CR2}} \leq 1$$

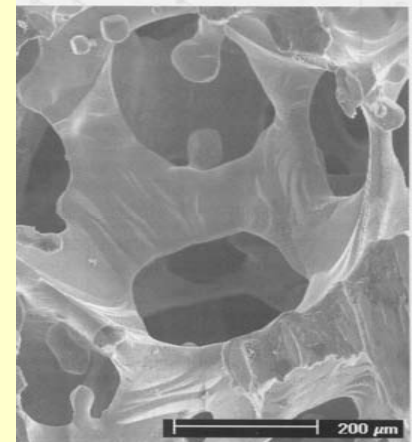
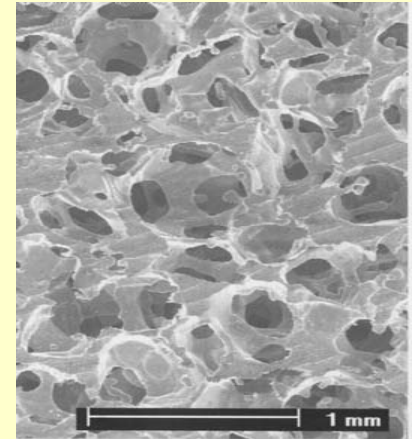
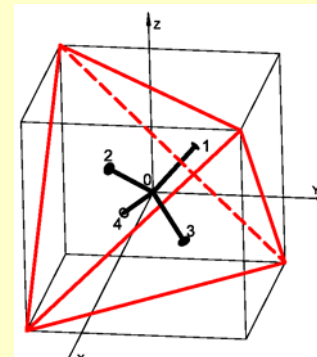
$$\Phi_{CR2} = \frac{1}{4G} (\underline{S}_{CR2} \cdot \underline{S}_{CR2})^2 = \frac{1}{G} R_e^2 \frac{16J^2}{3L^6 t^2}$$

$$\Phi_{CR1} = \frac{1}{2K} \sigma_{CR1}^2 = \frac{1}{2K} R_e^2 \cdot \left(\frac{4A}{\sqrt{3}L^2} \right)^2 = \frac{2}{K} R_e^2 \cdot \phi^2$$

C.San Marchi

A. Mortensen

Acta Metall.,
2001





Division of Applied Plasticity

Head: Prof. Wojciech K. NOWACKI

Thermo-mechanical modelling:

- **constitutive description,**
- **numerical identification & verification**

Materials: steels, Dual Phase (DP) steel, TRIP steel,
intermetallics

Experimental investigations:

- Simple shear tests at different strain rates from
- 10^{-3} s^{-1} to 10^4 s^{-1}
- Compression and tension tests at different strain rates from 10^{-3} s^{-1} to 10^3 s^{-1}
- Taylor test
- $K_{\text{id}}(t)$, crack propagation velocity
- Damage in brittle materials
- Ductile fracture

Materials: steels, polymers, SMA, composites

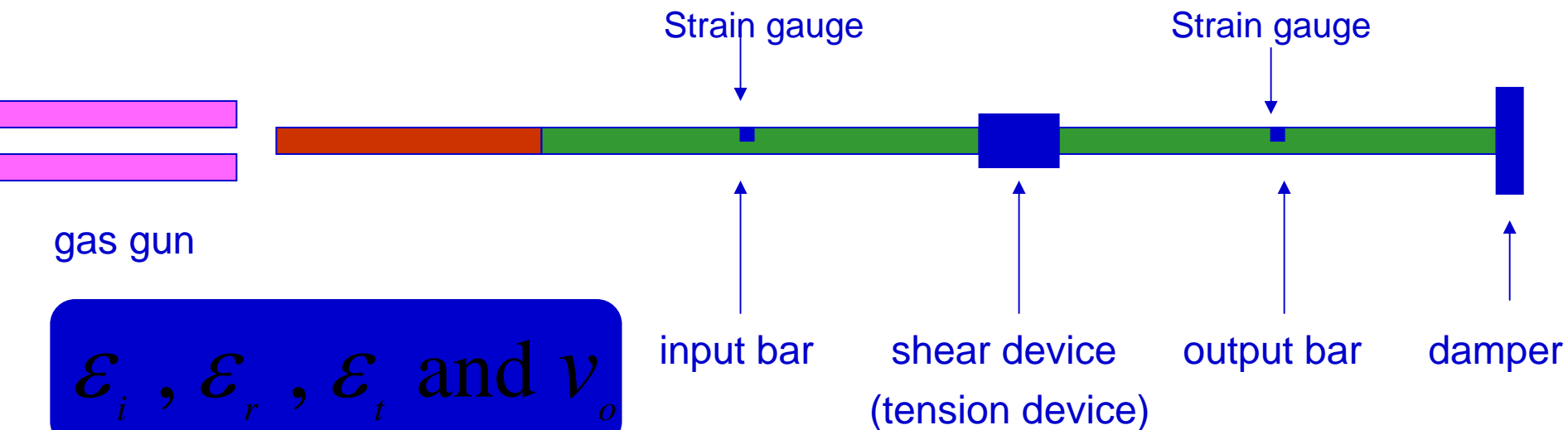
Laboratory Equipment



Testing machine 25 kN and the compression split Hopkinson bar facility

I. Compression Split- Hopkinson Pressure Bar (SHPB) scheme

dynamic experiment: a) simple shear
 b) tension



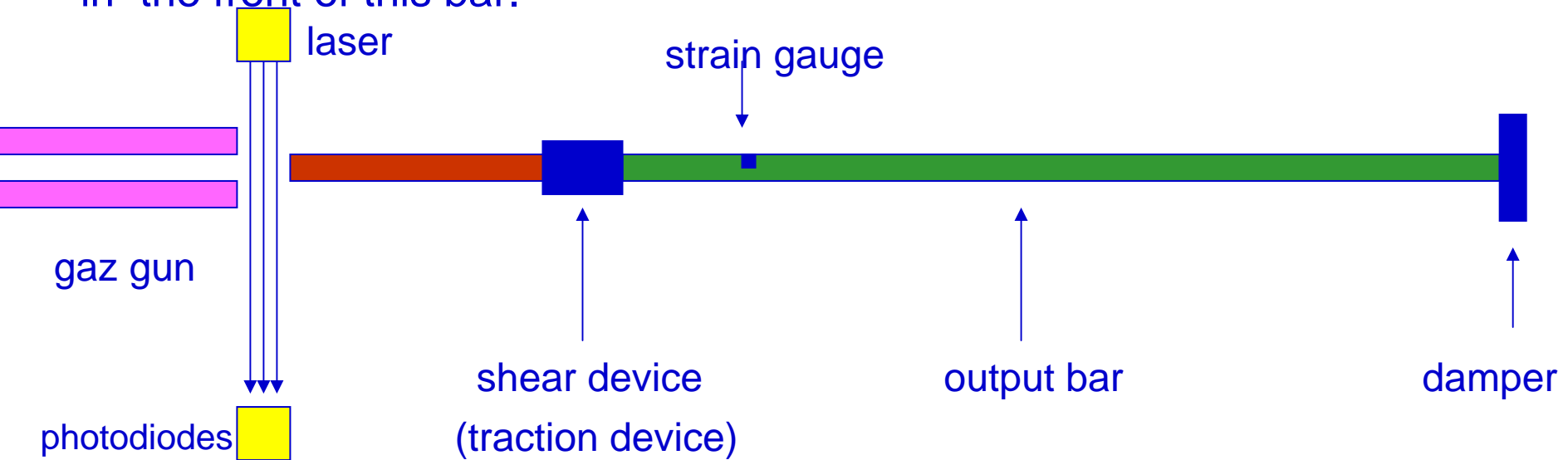
IMPORTANT: The mechanical impedance of two parts of the shear device and SHPB are the same.

$$\rho_D, A_D \Leftrightarrow \rho_{SHPB}, A_{SHPB}$$

II. Schematic of configuration of experimental set-up for direct impact:

a) simple shear test b) tension test

We use the transmitted bar only and the shearing (tension) device is placed in the front of this bar.

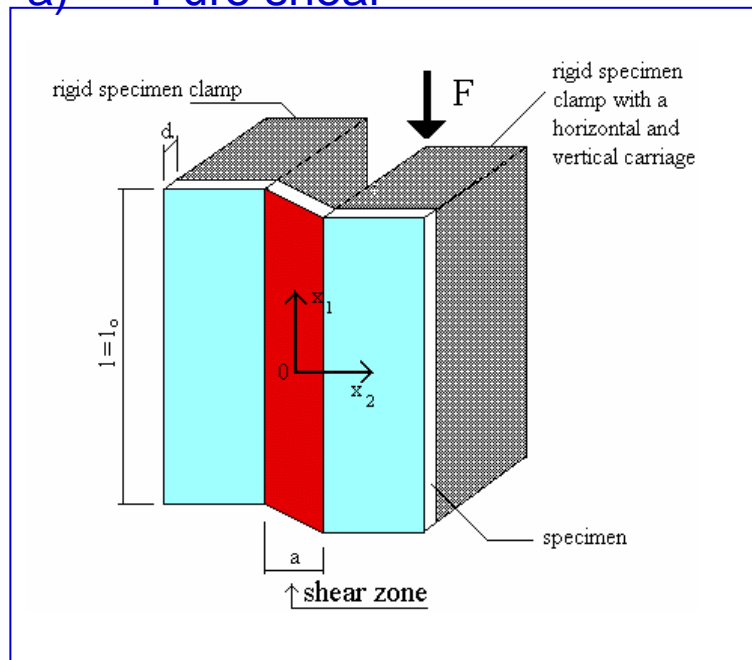


$$v_o, \epsilon_t$$

$$\rho_D, A_D \Leftrightarrow \rho_{SHPB}, A_{SHPB}$$

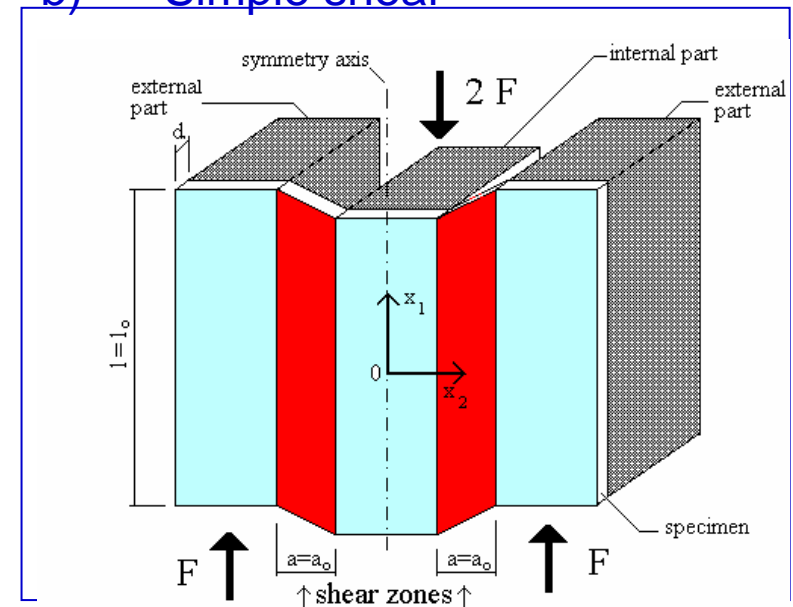
In the static investigations of the thin sheets we can distinguish two approaches, based on different principles of the shear device.

a) Pure shear

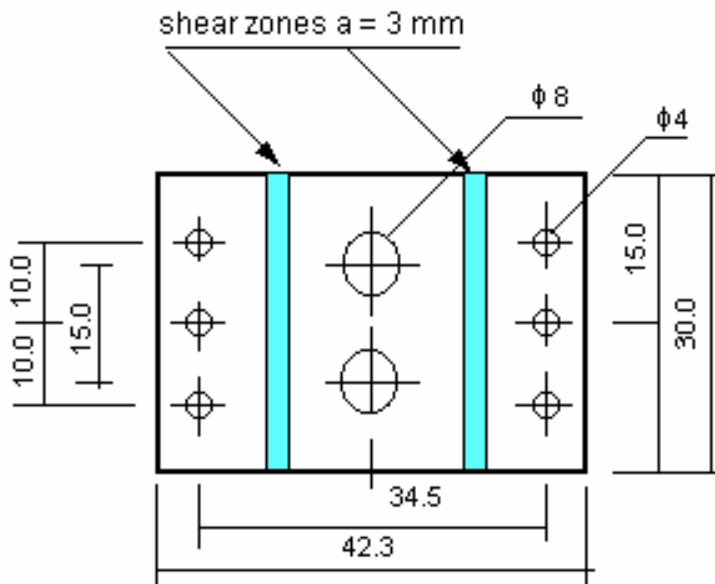


Shear device of the one shear zone only
proposed by G'Sell (1983)

b) Simple shear



Shear device for „double shear” specimens
proposed by Myauchi (1978)



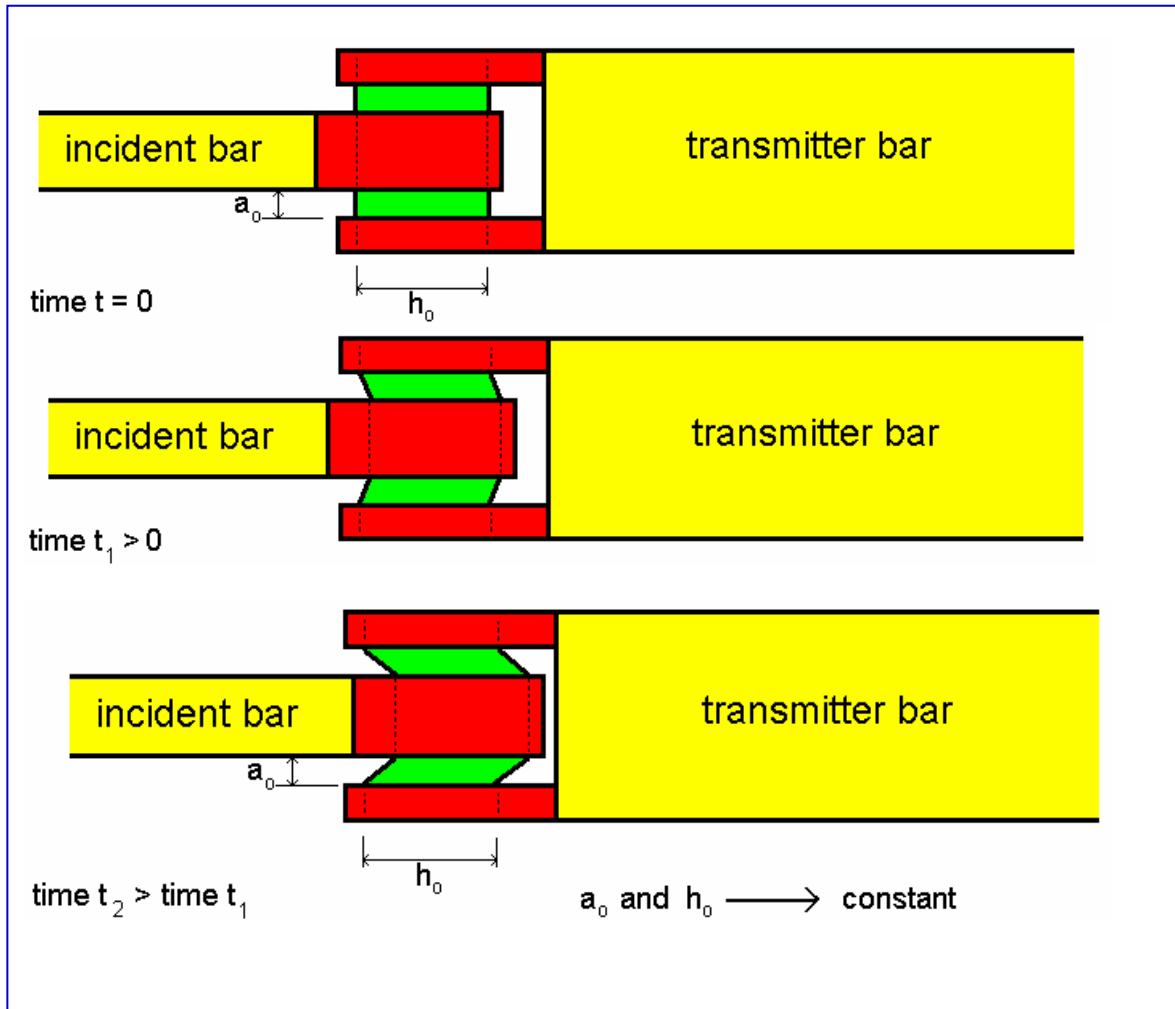
double shear specimen
(thickness of $d=0.8$ mm)

The greatest double shear specimen height allowed by the shear device is $l_o = 30$ mm.

The width value a_o is chosen with a view to satisfying two requirements:

- the ratio a_o/d of the width to the thickness has to be small enough to avoid the buckling of the sheared zone ($a_o/d < 10$)
- the ratio a_o/l_o of the width to the height has to be sufficiently small to minimize the error due to the non homogeneity of the shear stress and strain at the two ends of the sample ($a_o/l_o < 1/10$).

Simple shear - controlled by a SHPB acting in compression



Device for high strain rate shear test

A compression split Hopkinson pressure bar facility at Thermoplasticity Laboratory (IPPT- Warsaw)



→ Bars of the diameter:

- 22 mm - steel
- 25mm steel and 40mm PA7

→ Tube of the diameter 40 mm

Diameter of the projectile 22 mm

- Simple shear tests
- Compression and tension tests
- Taylor test
- $K_{id}(t)$, crack propagation velocity
- Damage in brittle materials

A new compression split Hopkinson pressure bar

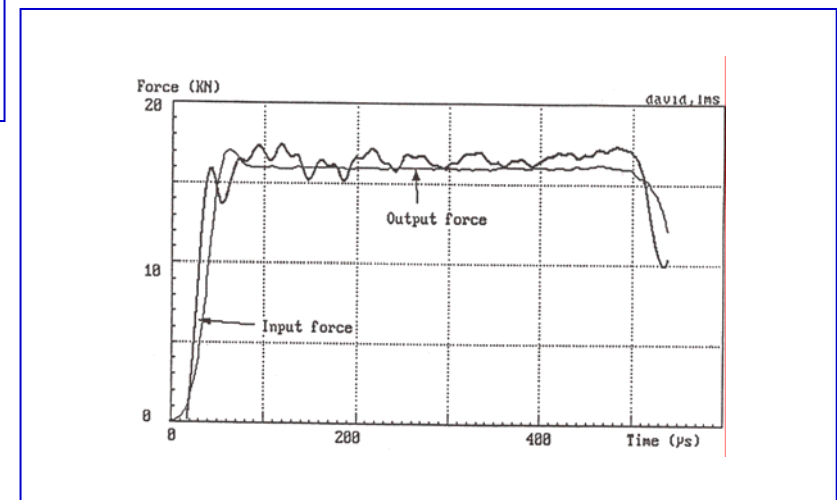
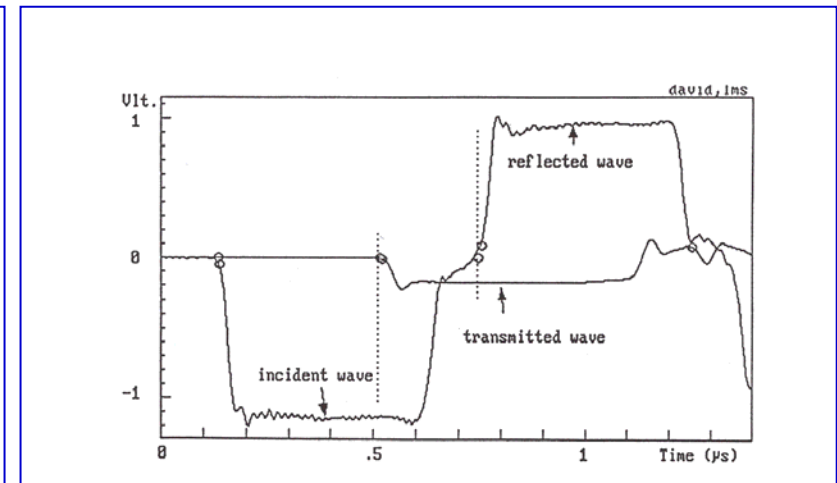
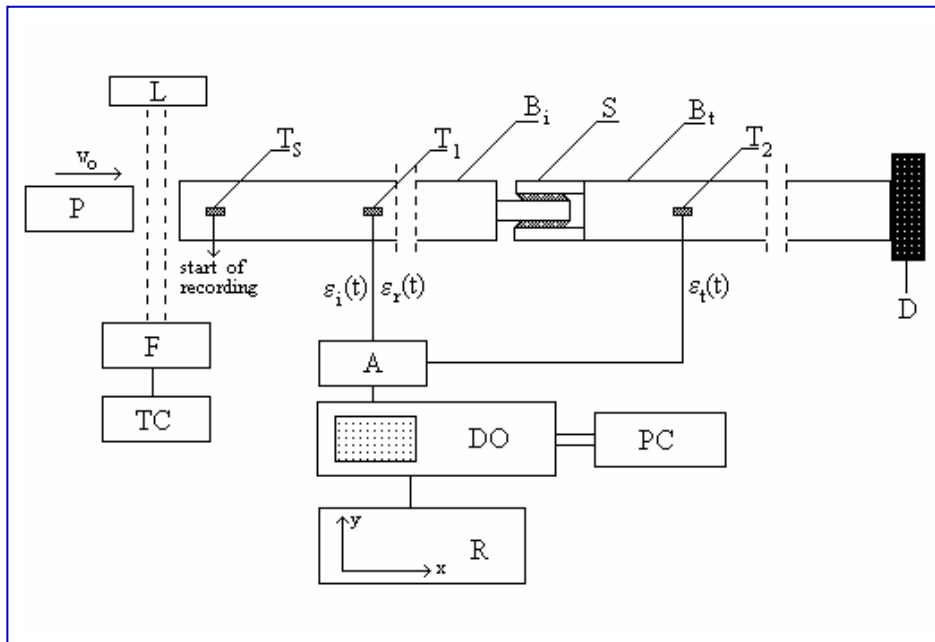


Bars of the diameter:

- 25 mm - steel
 - 25mm steel and 40mm PA7
- Tube of the diameter 40 mm and 60 mm

Diameter of the projectile 25 mm

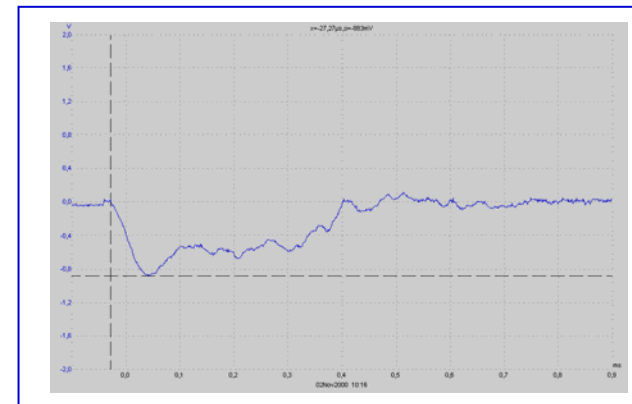
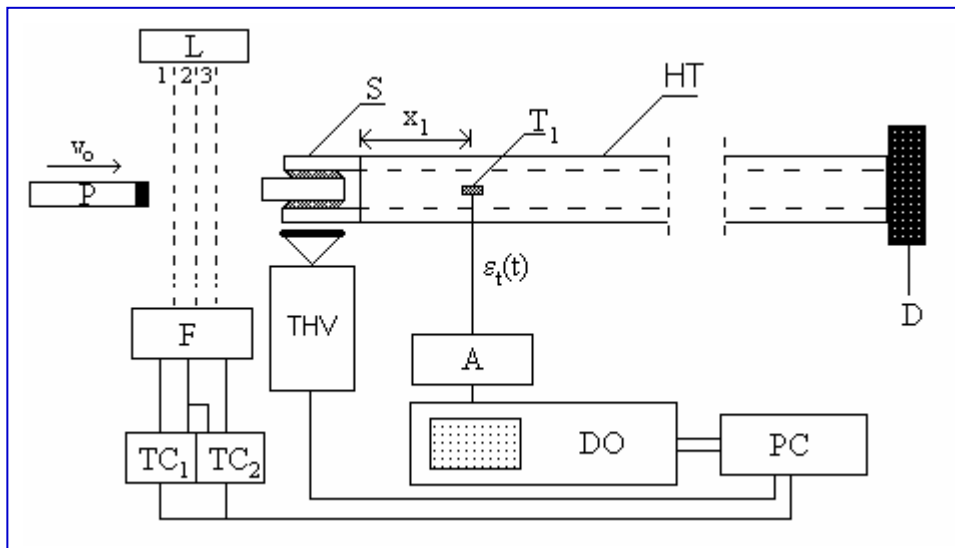
Simple shear in the classic configuration of compression SHPB



The input force and the output are very similar in shape.

Configuration of experimental set-up for direct impact – Hopkinson tube

Experimental stand at IPPT (Warsaw)



The temperature of the surface of the specimen can be measured only along one line.

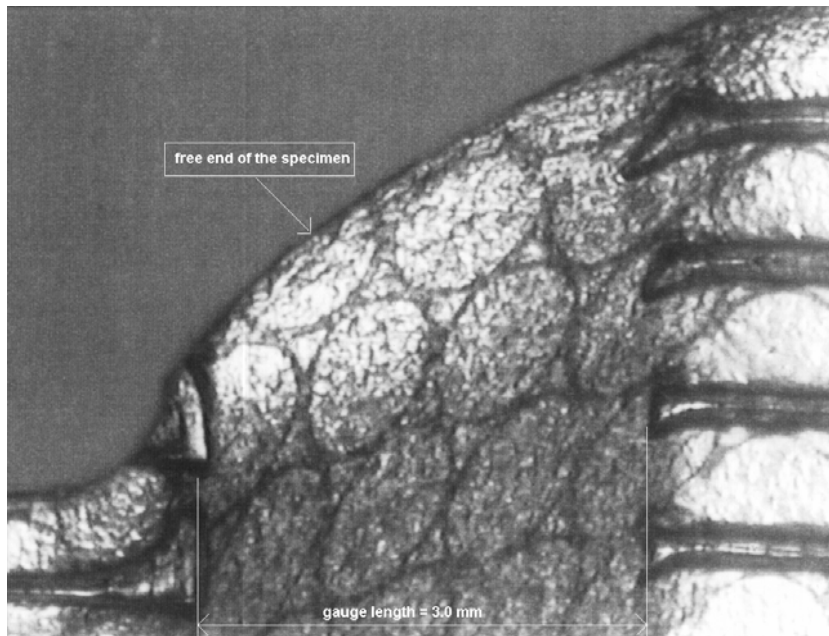
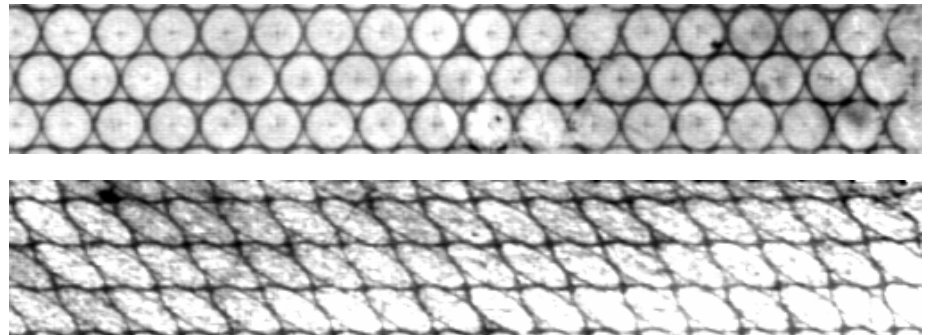
$$\bar{\gamma}(t) = \frac{1}{a_o} \left[v_o t - c_o \int_0^t \varepsilon_t(\tau) d\tau \right]$$

$$\dot{\bar{\gamma}}(t) = \frac{1}{a_o} [v_o - c_o \varepsilon_t(t)]$$

$$\bar{\sigma}_{12}(t) = \frac{S_T}{2S_E} E_o \varepsilon_t(t)$$

One of shear paths after dynamic simple shear at strain rate $3 \times 10^3 \text{ s}^{-1}$.

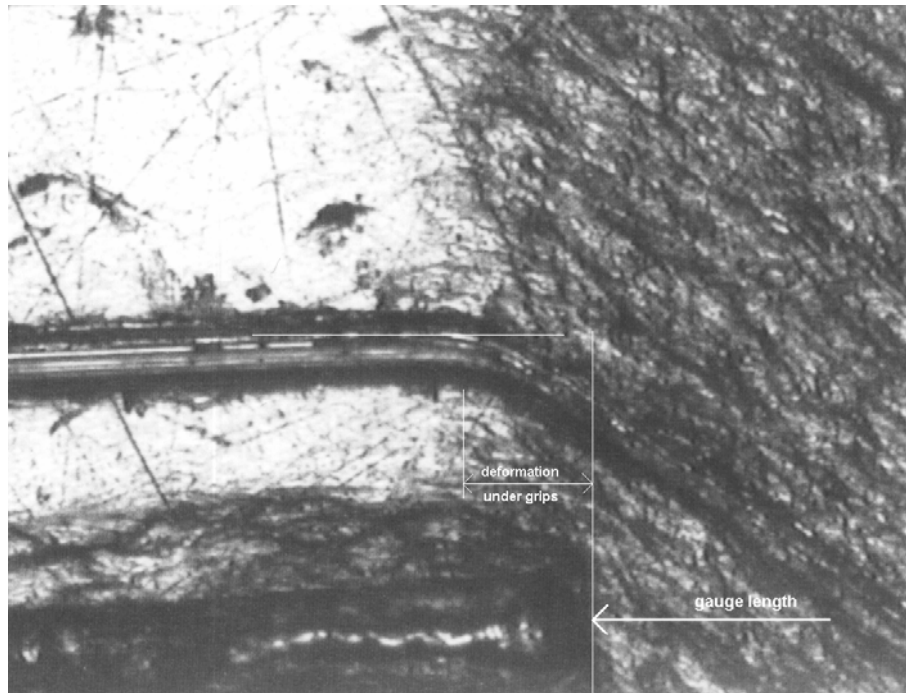
A photograph of the circular marking before (diameter of circles 1 mm) and elliptic after plastic deformation in simple shear up to 0.91.



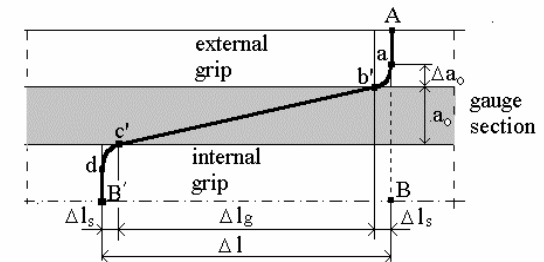
Within the central part of the shear zone 3.0mm the deformation field was quite uniform.

Free end of the specimen in simple shear.

One can observe the heterogeneity of the displacement field and important sliding under grips.



The layers under the grips are also partially deformed. The transversal straight lines marked on the specimen before the test, after deformation show small curved transition zones with the straight segment in the middle.



Relative axial displacement of the external and internal grips of the shear device is relatively easy to measure during the quasi-static deformation in the testing machine. It is a sum of two terms:

$$\Delta l = \Delta l_g + \Delta l_s$$

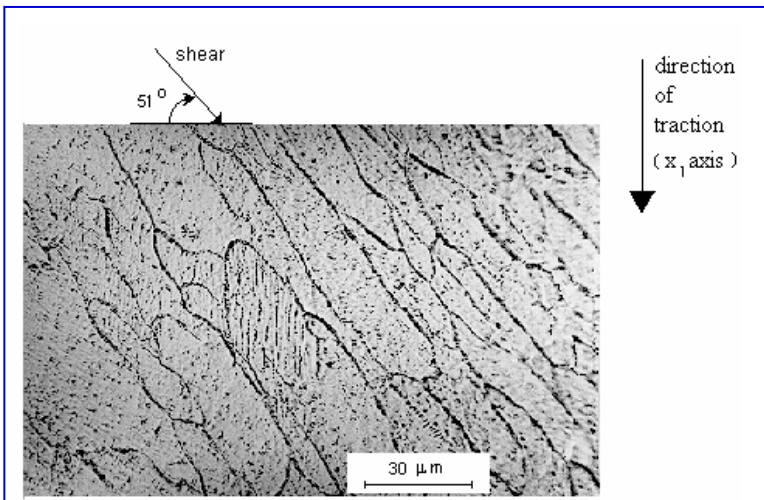
where Δl_s value of sliding under the grips.

Macro- and micro-bands of shear in the specimen

An essential feature is the formation of the tangled structure and of the dislocations cells. Their elongation and arrangement tend to be aligned along the shear direction.

At the very high strain rate the shear macro-bands are observed.

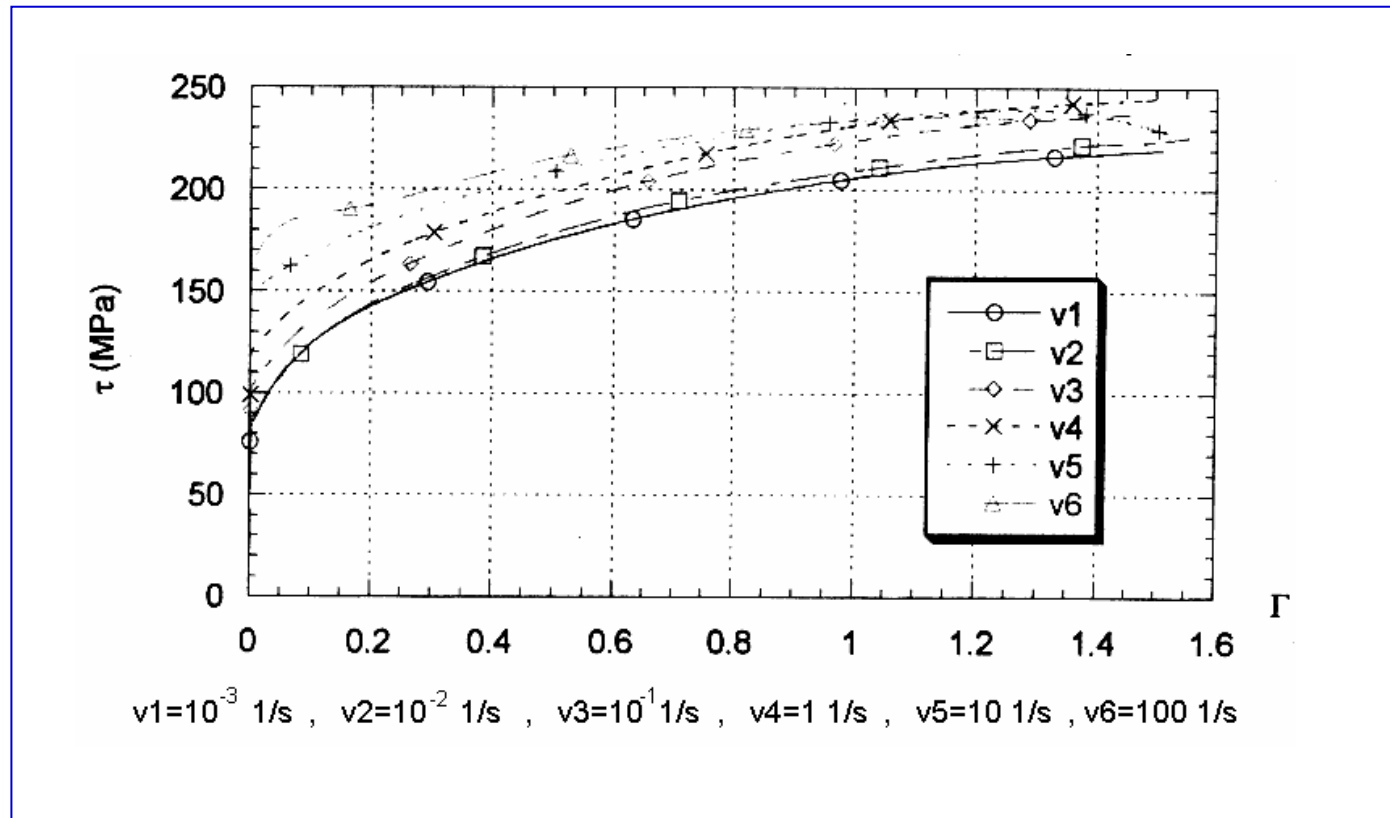
We can suppose that it is a critical strain at which the shear localization occurs. Before arriving at the critical strain, the deformation is homogeneous over the whole gauge length of the specimen.



Shear deformation of the order of 73%.

In several grains the micro-bands of shear parallel to the direction of x_1 axis are observed.

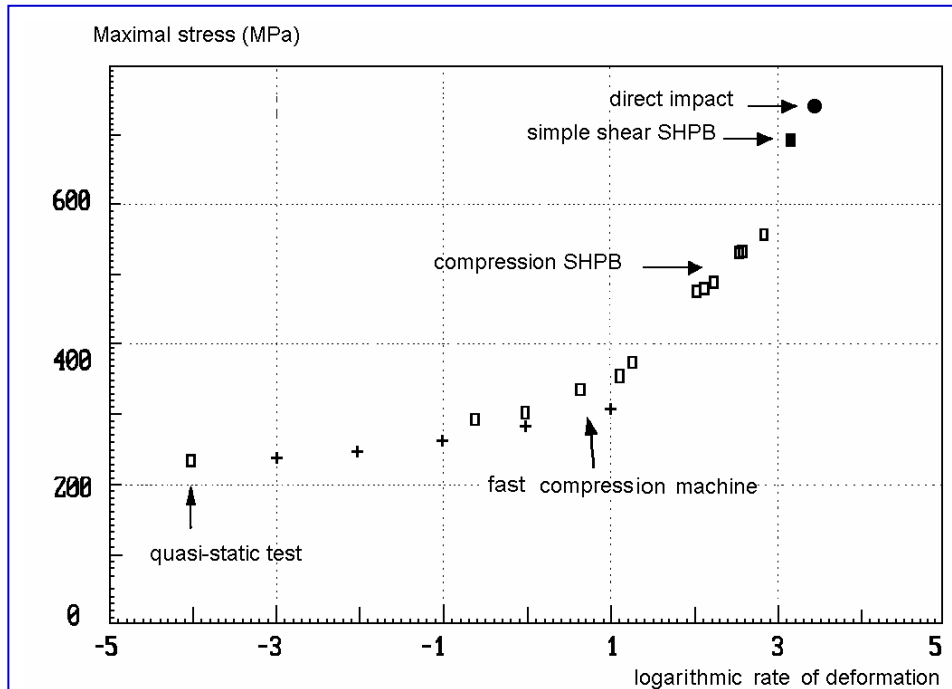
ES steel: C -50, Ni -25, Cr -18, Mn -189, Cu -23, Al -57, Si -4, P-17 in 10^{-3} volume percent



Shear stress – shear strain relations

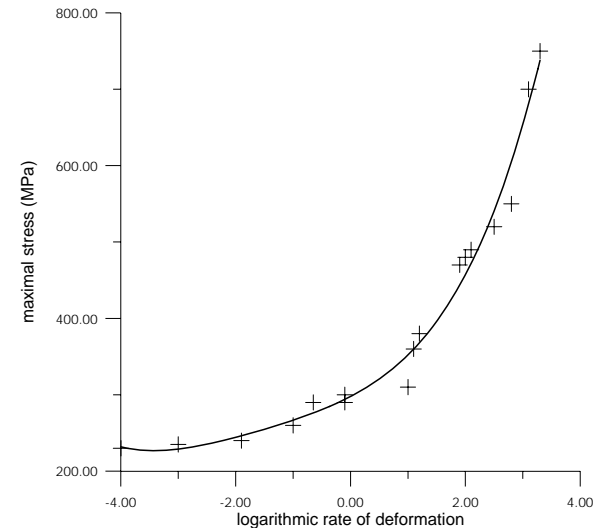
strain rates from 10^{-3} s^{-1} to 10^2 s^{-1}

Comparison of the simple shear test with the simple compression test for ES steel sheets.



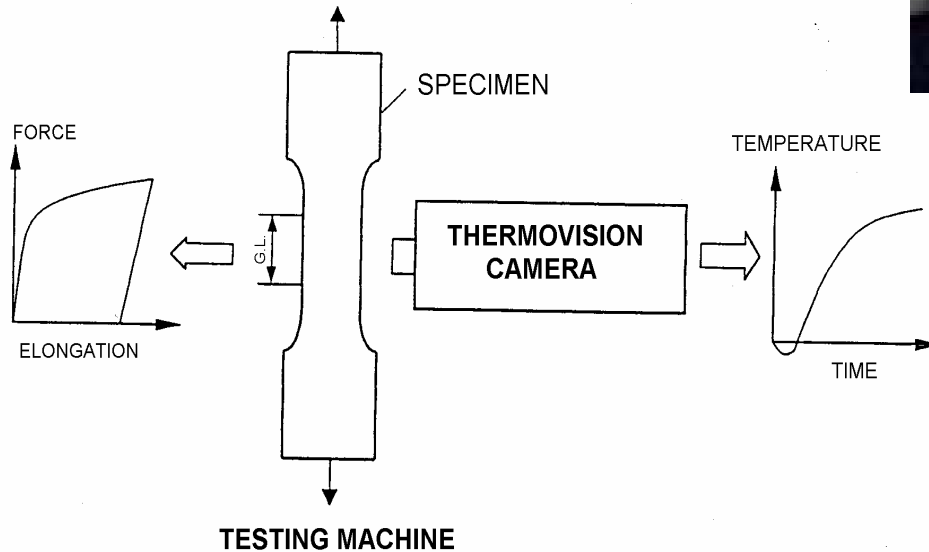
- quasi-static and dynamic test in compression
- simple shear: Gary and Nowacki (1994)
- + shear test in hydraulic machine
- direct impact: Klepaczko, Nguyen and Nowacki (1999)

Variation of the maximal stress versus logarithmic rate of deformation, for different kinds of experiments.



Rate sensitivity of the maximal stress for ES steel versus logarithm of shear-strain rate.

Hopkinson bar



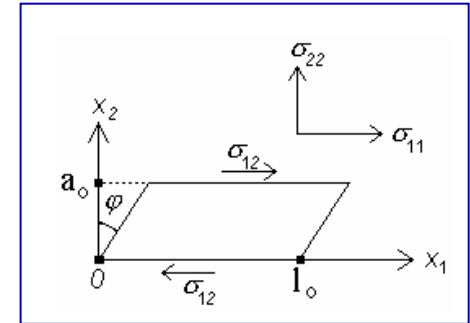
Thermographic set-
up to measure the
temperature
increase with
plastic deformation

Theoretical simple shear analysis

The simple shear in the direction \mathbf{e}_1 of the co-ordinate system $(\mathbf{e}_1, \mathbf{e}_2)$ is defined by the relations

$$u_1 = \gamma(t)x_2, \quad u_2 = u_3 = 0, \quad v_1 = \dot{\gamma}x_2, \quad v_2 = v_3 = 0,$$

where $\gamma = \tan \varphi$ - plastic shear strain, $\dot{\gamma}$ - shear strain rate.



$$\mathbf{V} = \frac{\dot{\gamma}}{2} \begin{pmatrix} 0 & 1 \\ 0 & 0 \end{pmatrix} \quad \mathbf{D} = \frac{\dot{\gamma}}{2} \begin{pmatrix} 0 & 1 \\ 1 & 0 \end{pmatrix} \quad \boldsymbol{\omega} = \frac{\dot{\gamma}}{2} \begin{pmatrix} 0 & 1 \\ -1 & 0 \end{pmatrix} \quad \boldsymbol{\sigma} = \begin{pmatrix} \sigma_{11} & \sigma_{12} \\ \sigma_{21} & \sigma_{22} \end{pmatrix} \quad \boldsymbol{\Pi} = \begin{pmatrix} \pi_{11} & \pi_{12} \\ \pi_{21} & \pi_{22} \end{pmatrix}$$

$$\check{\mathbf{T}} = \beta \mathbf{L} \mathbf{D} - \frac{3j\mu\beta \mathbf{D} \cdot (\bar{\mathbf{T}} - \boldsymbol{\Pi})}{\sigma_y^2 \mathbf{H}} [(\bar{\mathbf{T}} - \boldsymbol{\Pi}) + \mathbf{P}]$$

$$\beta = \rho_o / \rho$$

$$j = \begin{cases} 1 & \text{if } f = 0 \text{ and } \mathbf{D} \cdot (\bar{\mathbf{T}} - \boldsymbol{\Pi}) \geq 0, \\ 0 & \text{if } f = 0 \text{ and } \mathbf{D} \cdot (\bar{\mathbf{T}} - \boldsymbol{\Pi}) < 0 \text{ or } f < 0. \end{cases}$$

where $\mathbf{T} = \beta \boldsymbol{\sigma}$, $\beta = \rho_o / \rho$, $\check{\mathbf{T}} = \dot{\mathbf{T}} - \boldsymbol{\omega} \mathbf{T} + \mathbf{T} \boldsymbol{\omega}$

Huber-Mises-Hencky yield criterion:

$$f = \frac{3}{2}(\bar{\mathbf{T}} - \Pi) \cdot (\bar{\mathbf{T}} - \Pi) - \sigma_Y^2(\mathcal{G}, \alpha) = 0$$

Where σ_Y is the yield stress in simple tension, \mathcal{G} is the temperature and α corresponds to the size of the yield surface: $\dot{\alpha} = (\bar{\mathbf{T}} - \Pi) \cdot \mathbf{D}^P$.

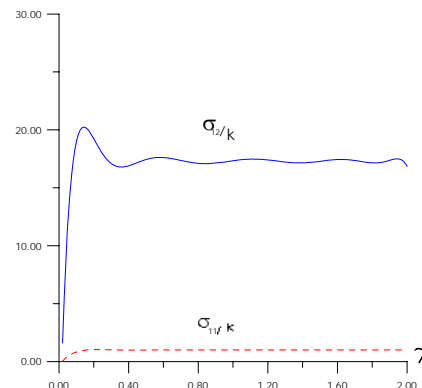
The change of temperature is described as:

$$\rho_o c_v \dot{\mathcal{G}} = (1 - \pi)(\bar{\mathbf{T}} - \Pi) \cdot \mathbf{D}^P$$

The term on the right hand side represents the rate of energy dissipation and, therefore, $\pi < 1$. For numerous metals π takes the value from 0.02 to 0.1.

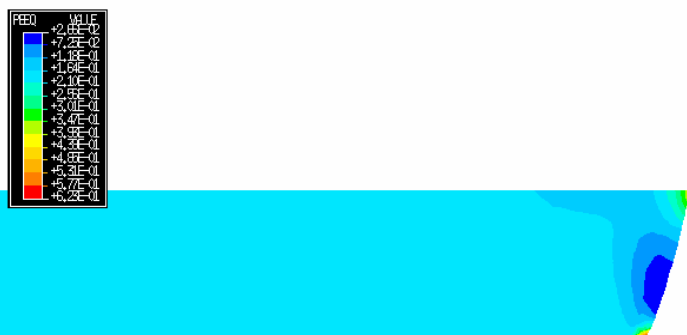
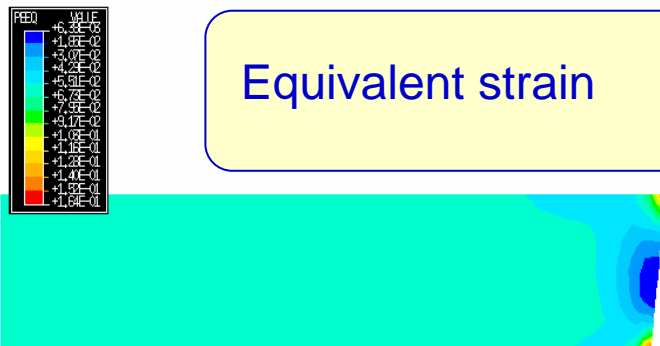
For plasticity with kinematic hardening

$$H = 1 + \frac{c}{2\mu}$$



Numerical simulation of the experiment – quasi-static deformation at 10^{-3} s^{-1}

Equivalent strain



Adiabatic shear bands – ES steel (French Standards)

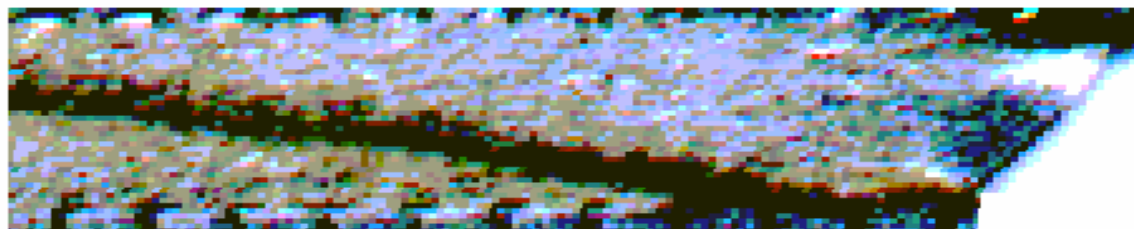
strain rate – 10^{-3} s^{-1}

shear strain 91.2 %



Results of numerical simulation.

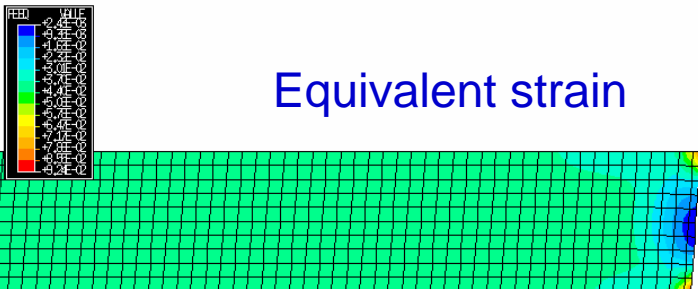
(1/2 of the specimen in simple shear)



Experiment

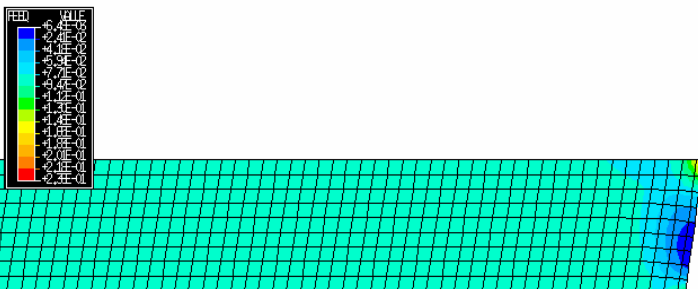
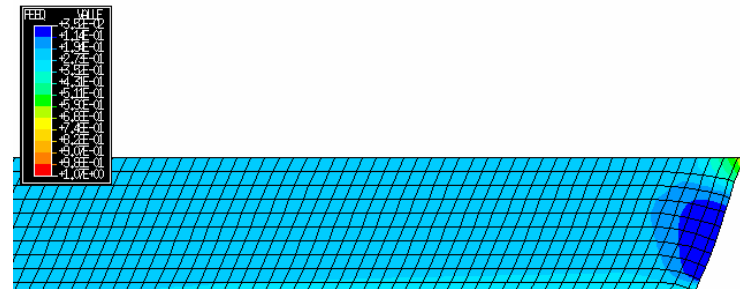
Numerical simulation of the experiment – dynamic deformation at 10^3 s^{-1}

Equivalent strain



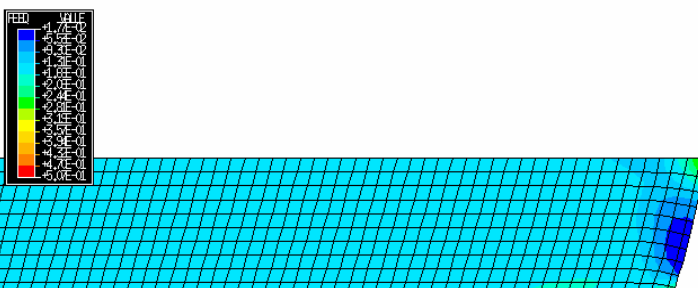
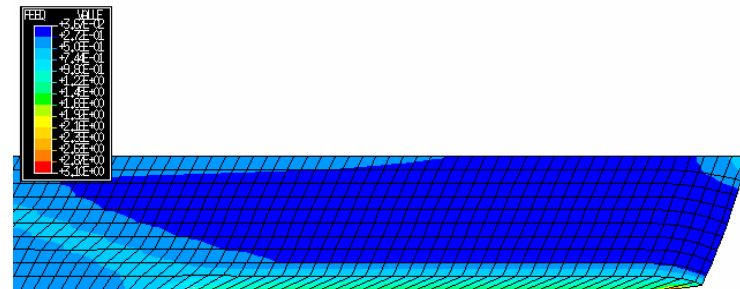
$\gamma=5.1\%$,

$\gamma=27\%$



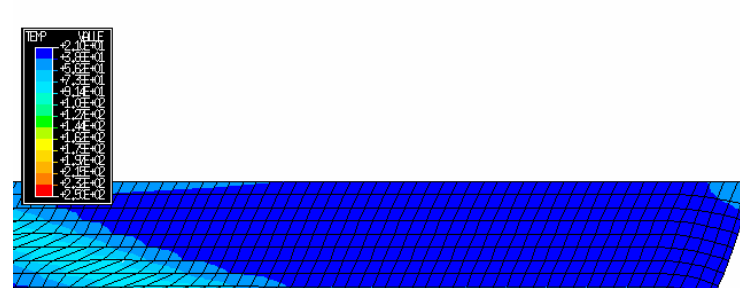
$\gamma=9.0\%$,

$\gamma=52\%$

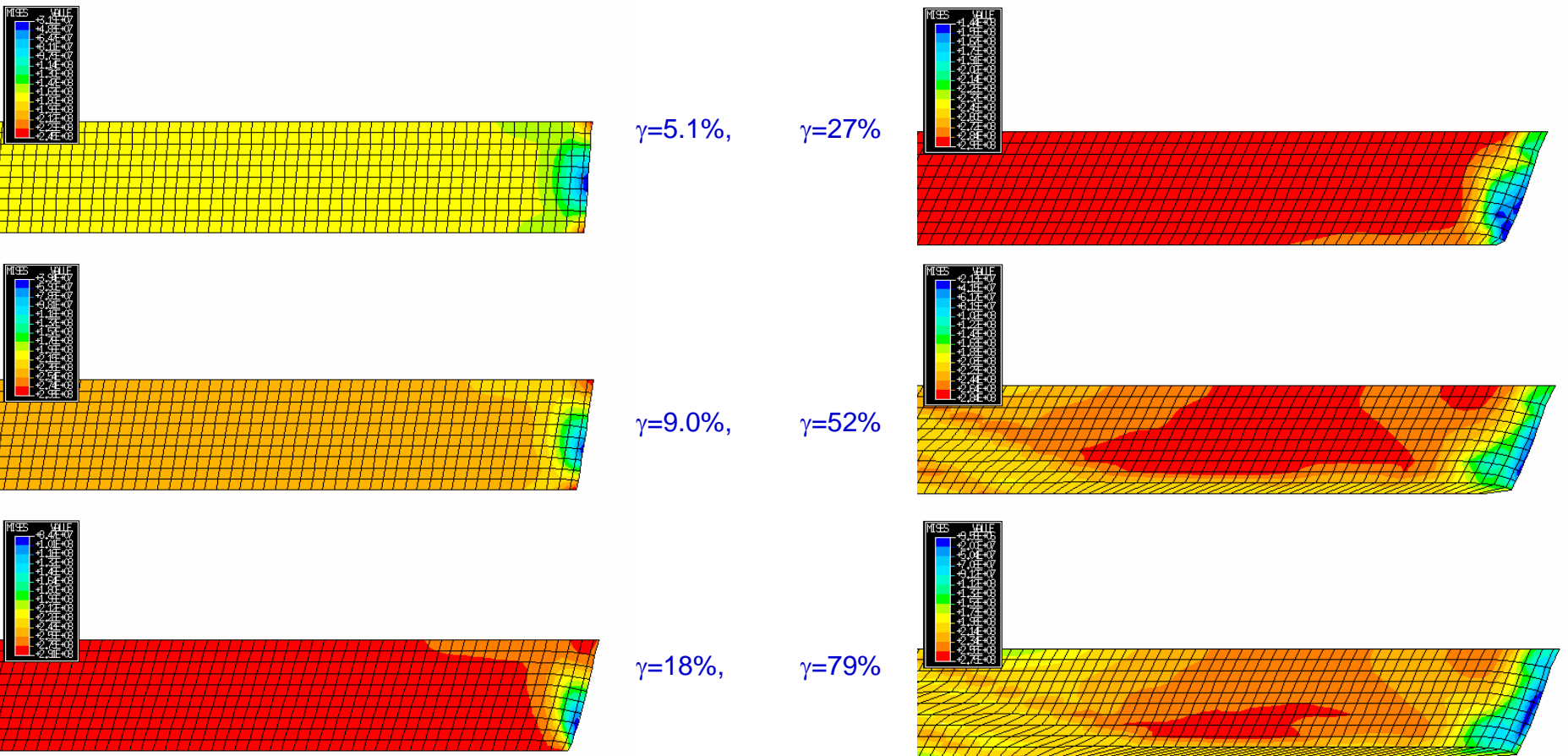


$\gamma=18\%$,

$\gamma=79\%$



Numerical simulation of the experiment – dynamic deformation at 10^3 s^{-1}



Equivalent stress

Conclusions from numerical simulation of the experiment

Quasi-static case:

One can observe the heterogeneity of the strain and stress fields at the ends of the specimen, at the distance less than 1.7% (accurate to 10^{-4} of deformation) of the total length when the mean strain is 0.3, and less than 6.6% when the strain is 0.7. We observe the formation of the shear band.

Dynamic case:

- Contrary to the quasi-static deformation, the beginning of the localization in the dynamic case occurs at lower shear strains. A distinct shear band appears in the middle part of the shear zone with inclination $\phi = 51^\circ$ to the x_1 axis. In addition, an intense shear strain is observed in the specimen and the support areas of the shear device.
- Numerical calculations were not conducted for advance localization, when the results are mesh-sensitive.
- The performed numerical calculations enabled us to evaluate the optimal dimensions of the double shear specimen.



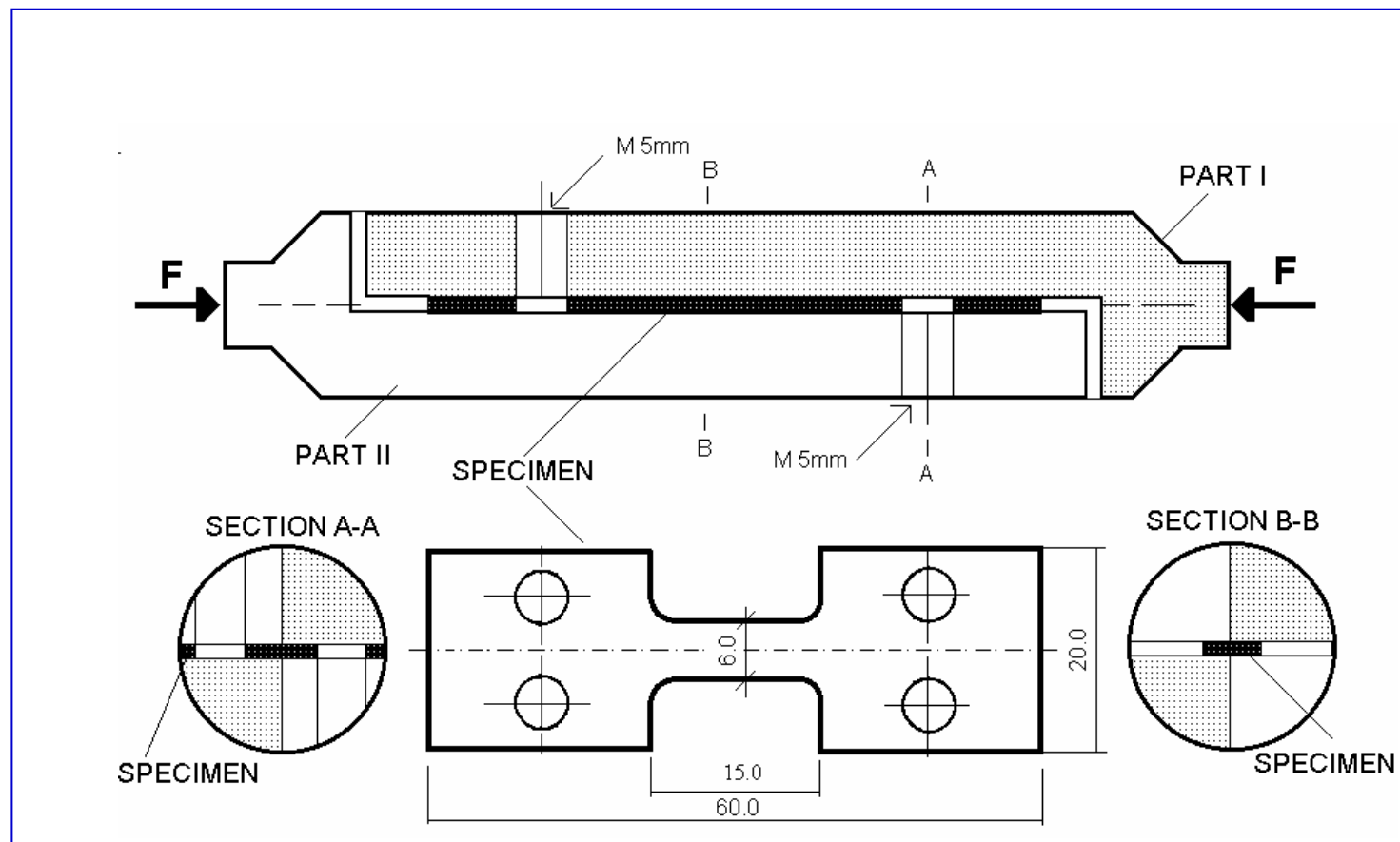
Tension device in testing machine

A new tension device was used by us to perform tests at high strain rates on specimens made of metal sheets.

The loading and the displacements of this device are controlled by SHPB acting in compression.

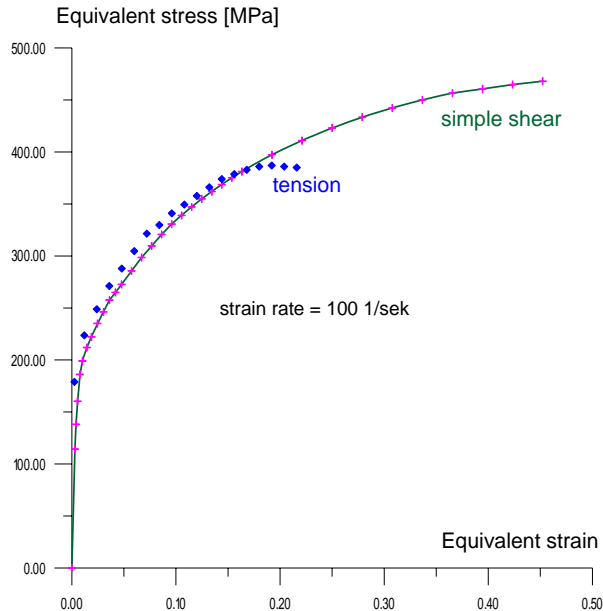
The role of the special device is to transform the compression into tension (inversion of motion).

The mechanical impedance of two parts of the shear device and SHPB are the same.



Device for high strain rate tension tests

Comparison of simple shear test with tension test



The comparison of the result obtained in the simple shear test and tension test for ES steel at strain rate 100 s^{-1} . We assume the Huber-Mises-Hencky yield criterion: $\gamma = \sqrt{3}\varepsilon_{11}$ and $\sigma_{12} = \sqrt{3}\sigma_{11}$.

The influence of stress components σ_{11} and σ_{22} must be taking account.

The stress intensity is defined as:

$$\sigma_i = [\sigma_{11}^2 + \sigma_{22}^2 + 3\sigma_{21}^2 - \sigma_{11}\sigma_{22}]^{1/2}$$

CONCLUSIONS

- Considerable homogeneity of the permanent strain field at finite deformations over the total length of the specimens is observed in experiments of simple shear and in the results of simulation.
- The proposed method is the only known test providing, in the case of a thin sheet, homogeneous stress and strain fields in both the dynamic and static tests.
- Simple shear test is particularly attractive, since the application of this type of loading path can result in large strains without the occurrence of plastic instability.